# Real Time Process Monitoring of Solder Paste Stencil Printing

by

## Daniel J. Braunstein

Submitted to the Department of Mechanical Engineering
in partial fulfillment of the requirements for the degree of

Master of Science in Mechanical Engineering

at the

MASSACHUSETTS INSTITUTE OF TECHNOLOGY

February 1994

Author .................................................................
Department of Mechanical Engineering
February 17, 1994

Certified by .................................................................
Haruhiko Asada
Professor of Mechanical Engineering
Thesis Supervisor

Accepted by .................................................................
Ain A. Sonin
Chairman, Department of Graduate Committe
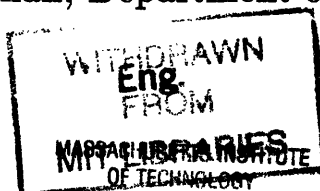
# Real Time Process Monitoring of Solder Paste Stencil Printing

by

Daniel J. Braunstein

Submitted to the Department of Mechanical Engineering
on February 17, 1994, in partial fulfillment of the
requirements for the degree of
Master of Science in Mechanical Engineering

## Abstract

A new approach to printing process control is presented. Innovative methods for manufacturing process control will be developed, using techniques which have previously been exclusively applied in classical and modern control theory.

This thesis develops a model for the fluid motion induced during the printing operation, and describes appropriate techniques for *in-situ* process monitoring. A model in which measureable quantities and actuated signals were linearly related to unknown parameters was derived. These parameters reflected the properties of the solder paste and were estimated in real time using recursive least squares algorithms. Results of the estimation are presented for a linear and nonlinear model.

Thesis Supervisor: Haruhiko Asada
Title: Professor of Mechanical Engineering

# Acknowledgments

# Contents

# List of Figures

6

# Chapter 1

# Introduction

## 1.1 Background

The development of surface mount microelectronic devices (SMDs) was the electronic industry's solution to consumer demands for highly reliable packages with improved performance, increased functionality, and decreased size. Recent advances, such as the production of devices with as many as 500 leads and pitches as small as 0.3 mm has furthermore forced the industry to devise and improve certain surface mount assembly processes. For instance, many chip placement machines currently perform the pick and place operation at a rate of over ten components per second; while soldering methods have evolved from wave to reflow technology, permitting thermally sensitive components with complex lead geometries to be soldered with fewer defects and improved electrical characteristics [1]. However, unlike placement, reflow, and many other processes, where the technology used for surface mount assembly has matched or surpassed demands for high performance and reliability, the application of solder paste via stencil printing has remained a rudimentary procedure. Although proper paste deposits alone cannot guarantee defect-free solder joints, the application of paste with sufficient pad coverage, uniform height, and favorable slumping characteristics is a necessary condition. Stencil printing is the first of many processes in SMD assembly where enhanced process control techniques will aid in the avoidance of defects such as bridges, solder balls, and voids.

8

## 1.2　Quality of Solder Joints

Since the quality of solder joints is a function of the interactions among solder paste, manufacturing equipment, and the environment, numerous studies have focused on characterizing the physical behavior of paste and how its properties affect printability and solderability [2], [3], [4]. Most of these efforts have relied on off-line experimental methods for process optimization, employing techniques such as the Taguchi method and full factorial experiments [5], [6]. Although these approaches have helped improve certain operations, they do not completely resolve or address many assembly issues. The primary reason that these methods are unsatisfactory, is that paste properties vary during assembly processes. Solder paste solvents evaporate as a function of time, temperature, and humidity, causing oxidation and other unfavorable conditions. Furthermore, mechanical properties, such as viscosity and elasticity, change with exposure to the environment as well as with the amount of work applied to the paste, *e.g.* squeegee speed and duration of print. These changes to the paste adversely affect joint quality and frequently require adjustment of assembly equipment to maintain product quality and throughput at tolerable levels. The retuning procedure is time consuming, costly, and requires human expertise. New methods must be devised for *in-situ* material characterization for the purposes of closed loop control. Control actions should occur dynamically is accordance with measurements which characterize real time changes to material properties, rather than occurring on an *ad-hoc* run-by-run basis. Not only will real time monitoring and closed loop control lead to improved process performance and product quality, but will also minimize time required for post process inspection, since feedback is also achieved through *in-situ* sensor signals.

## 1.3　Material Estimation for Improved Joint Quality

On-line material characterization is crucial if appropriate control actions are to be performed. However, the relevant material properties must be identified for particular

processes. For example, identification of the viscoelastic properties of the paste are necessary to determine printing parameters such as squeegee speed, angle, downward force, and snap-off; while chemical, thermal, and electrical characteristics may be more relevant for control of reflow temperature profiles. There is certainly a coupling among the mechanical, chemical, and electrical properties, and any one property does not necessarily define the state of the paste for all assembly processes.

Until recently, no research had been conducted in the field of on-line monitoring of paste properties. The most relevant study explored the application of impedance spectroscopy [7], [8]. This technique measures the electrical frequency response of solder paste by applying an oscillating voltage and measuring the corresponding current. In [7], [8] an equivalent circuit model of the paste was derived from experiments, and the values of various capacitances and resistances were determined and correlated to physical properties and phenomena occurring within the paste. Since electrodes are placed on a test pad on the printed circuit board, electrical impedance can be measured throughout the entire assembly process. However, [8] noted that electrode capacitance, electric field fringing, and surface effects make the measurements geometry dependent. Furthermore, measurements require consistent volumes of paste to be deposited onto the electrodes, which is one of the problems associated with the printing process. It is unclear how the electrical response relates to the mechanical and chemical behavior of the paste or how these signals can be used for process improvement, but nonetheless impedance spectroscopy may provide useful information in terms of creating new SPC variables.

The fundamental deficiency in any related research to date is that there has been a lack of understanding of the physics of the various assembly processes, and that there have been no attempts to couple material monitoring with a model based approach to real time process control.

# 1.4 Application to Stencil Printing

As previously stated, proper paste depositions are a necessary condition for acceptable solder joints. The focus of this research was to devise methods for on-line material characterization during paste printing. This process possesses all of the elements described above. Varying material properties make control difficult and time consuming, human expertise is required to operate the equipment and diagnose faults, and off-line experimental methods are currently relied upon for proper paste selection and tuning of the printing parameters. This approach to control and optimization *alone* is inadequate. Through modeling of the printing process as well as innovative measurement and actuation techniques, real time process monitoring can be achieved. Based on a model for the fluid motion during printing, a printing machine was instrumented with a two degree-of-freedom load cell which acquired *in-situ* force signals, describing the fundamental physics of the printing process and material properties.

Chapter 2 briefly describes the printing process and discusses the fluid behavior of solder paste. The fluid mechanics of the flow induced at the squeegee/stencil interface is explored in Chapter 3, and a similarity solution developed by Taylor [9], [10] is proposed for Newtonian flow. Analytical results for the streamline function, pressure, and shear rate distribution are calculated and compared to results obtained by [11] and [12]. Chapter 3 also includes a discussion of non-Newtonian corner flow. Based on the analysis in Chapter 3, Chapter 4 develops a model which includes friction, contact, and hydrodynamic forces. From preliminary results, an empirical non-linear is developed. An explanation of the monitoring algorithm is given in Chapter 5, along with estimation results for the linear and nonlinear models. Concluding remarks are contained in Chapter 6 and future endeavors are discussed.

# Chapter 2

# Stencil Printing and Paste Properties

Obtaining uniform paste deposits require accurate machine control and many appropriate design decisions, including paste and squeegee selection, stencil design, and operating set points of the printing machinery. Since there exists a plethora of relevant factors and the complex interactions among these factors is not well understood, modeling of the printing process is difficult. However, without some degree of modeling, whether complex analytical expressions or empirically derived parametric models, superior control of the printing process cannot be achieved.

Many studies in the field, notably [13]-[18], have attempted to describe the paste deposition process in a set of all encompassing equations. Although, these investigations have explained some of the mechanisms involved in paste printing, their approaches have not led to solutions which are altogether useful for material monitoring and control. For tractability of modeling, the process should be divided into logical *sub*processes. Neglecting procedures such as PCB loading and registration, the printing operation can be divided into the following operations.

1. *Gross paste flow by squeegee motion.*

2. *Flow into stencil apertures.*

3. *Paste transfer by stencil release.*

12

Gross paste motion is the motion of the paste in front of the squeegee during the printing operation. This motion is frequently referred to as the "rolling" of the paste bead. Study of the gross paste flow by virtue of squeegee motion is critical, since the generated hydrodynamic pressures will partially determine how paste fills stencil apertures. Other factors which dictate how paste flows into stencil openings include material properties, as well as aperture dimension, orientation, and wall roughness. The release of the paste onto the substrate is dominated by adhesion to aperture walls and copper footpads, as well as fluid surface effects during transfer. As a first step in understanding this complex process, primary attention has been directed toward modeling of the gross fluid motion, since sensor signals from this motion can readily describe material properties and physical phenomena occurring during the process.

## 2.1  Paste Characterization

Solder paste is a suspension of solder powder in a flux binder, containing additional additives to tailor certain characteristics, such as the ability of the paste to retain its shape, adhere to the substrate, and resist oxidation [19]. [6] indicated that selection of the paste largely depends on the pitch of the devices to be printed. Factors which influence the selection of a particular paste include the metallurgical composition, solids content, size and shape of the solder powder, and rheological characteristics, [20]. Ultimately, solderability of the paste is of concern. Joints must be produced with high conductivity and resistance to thermal fatigue and corrosion. Solderability is clearly a function of the type of solder used, but the quality of joints also depends on the soldering and application processes.

For paste printing, the most relevant rheological properties of the solder paste is its resistance to flow under an applied stress and its ability to retain its shape after stencil release. The resistance to fluid flow under an applied load is measured by the viscosity, while the ability of the flux binder to suspend the solder particles and retain its shape is governed by the fluid's elastic properties. The elastic properties of the fluid are important in small amplitude motions and high frequency excitation,

but the paste's viscous properties are the dominant factors for rolling motion. For this reason, elastic effects were neglected and the paste was treated only as a viscous fluid.

For a special type of fluid, called a *Newtonian fluid*, the stress tensor, $\tau$, is proportional to the rate of strain tensor, $\dot{\gamma}$, and is given by,

$$\tau = \mu\dot{\gamma} \tag{2.1}$$

where the viscosity $\mu$, is the constant of proportionality. Analytical solutions to many Newtonian viscous flow problems with various boundary conditions can be derived. Unfortunately, solder paste exhibits non-Newtonian behavior; that is, the stress in the fluid is a nonlinear function of the rate of strain. For such fluids, the viscosity is often described by either the apparent viscosity, $\mu_a$, or the differential viscosity, $\mu_\delta$, where the apparent viscosity is the ratio of the stress to strain rate, and the differential viscosity is the instantaneous slope relating $\tau$ and $\dot{\gamma}$. For flows where the viscosity is a function of rate of shear, the relation describing the stress and the shear rate can be written as

$$\tau = \mu(\dot{\gamma})\dot{\gamma} \tag{2.2}$$

where $\mu(\dot{\gamma})$ emphasizes that the viscosity for this flow is a function of the rate of strain. Although the concept of generalized Newtonian flow is useful in describing certain fluid behavior, [21] noted that this description is limited because it cannot explain time dependent phenomena associated with viscoelasticity. Nonetheless, empirical relationships have been established relating the shear and strain rate for many flow problems.

The non-Newtonian characteristics of solder paste can be described by the following power law relation for viscosity,

$$\mu(\dot{\gamma}) = k\dot{\gamma}^{(n-1)} \tag{2.3}$$

Here $k$ is a measure of the thickness of the fluid and the exponent $n$ is a measure
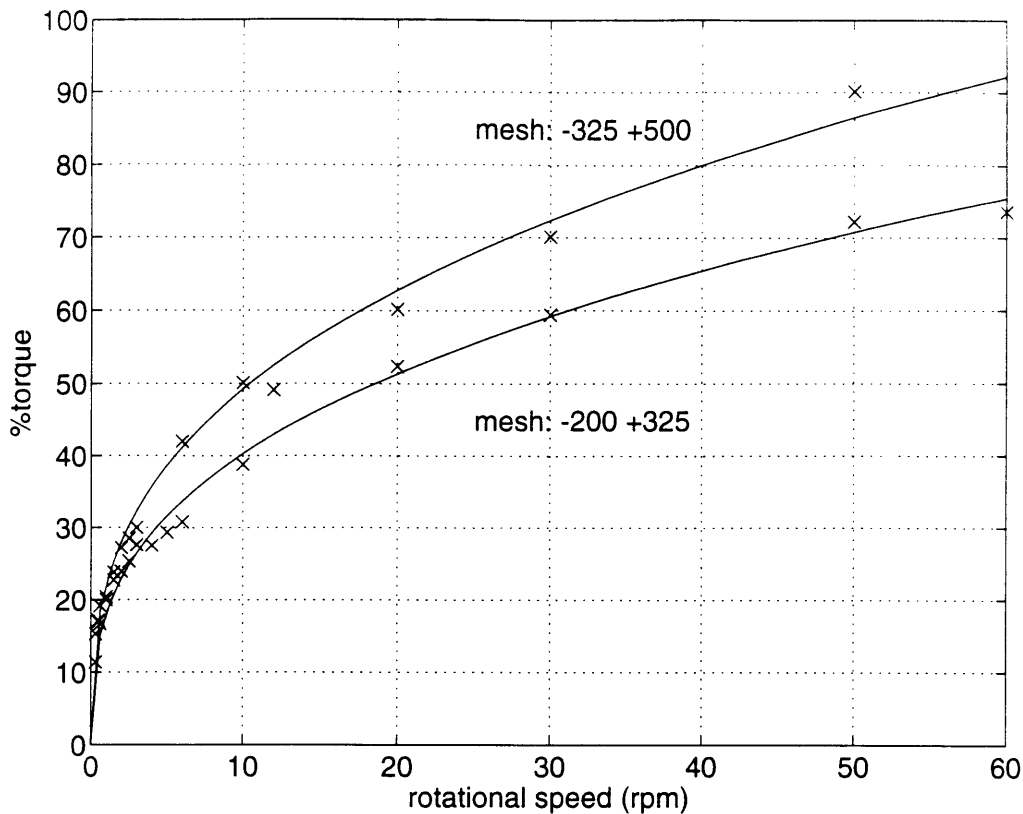
Figure 2-1: Stress and shear rate curves for solder paste.

of the non-Newtonian characteristics. For $n = 1$, the fluid equation collapses to the Newtonian relation in Equation 2.1. Typically, for high strain rates, $n$ approaches unity, and over this range the fluid can be described by Equation 2.1, with the inclusion of an intercept term. Data acquired from a Brookfield rotational viscometer in Figure 2-1 displays the non-Newtonian characteristics of two types of solder paste as indicated. Shear was measured as the percent of the motor torque, and shear rate as spindle rpm. Tests were conducted using a Brookfield DVII+ viscometer with RV spindle number 7. The non-Newtonian flow behavior will be discussed in Chapter 3.

Another property of the solder paste which makes analysis difficult, is that the fluid displays time dependent behavior, referred to as *thixotropic* behavior. The term *thixotropic* is used generically to describe any time dependent variation of the paste properties. For a thixotropic fluid, the time of applied shear will alter the apparent viscosity of the paste. This phenomenon, called shear thinning, is most similar to work hardening or softening frequently encountered in fatigue tests of metal specimens. If a thixotropic fluid undergoes constant shear rate, the apparent viscosity will vary

15
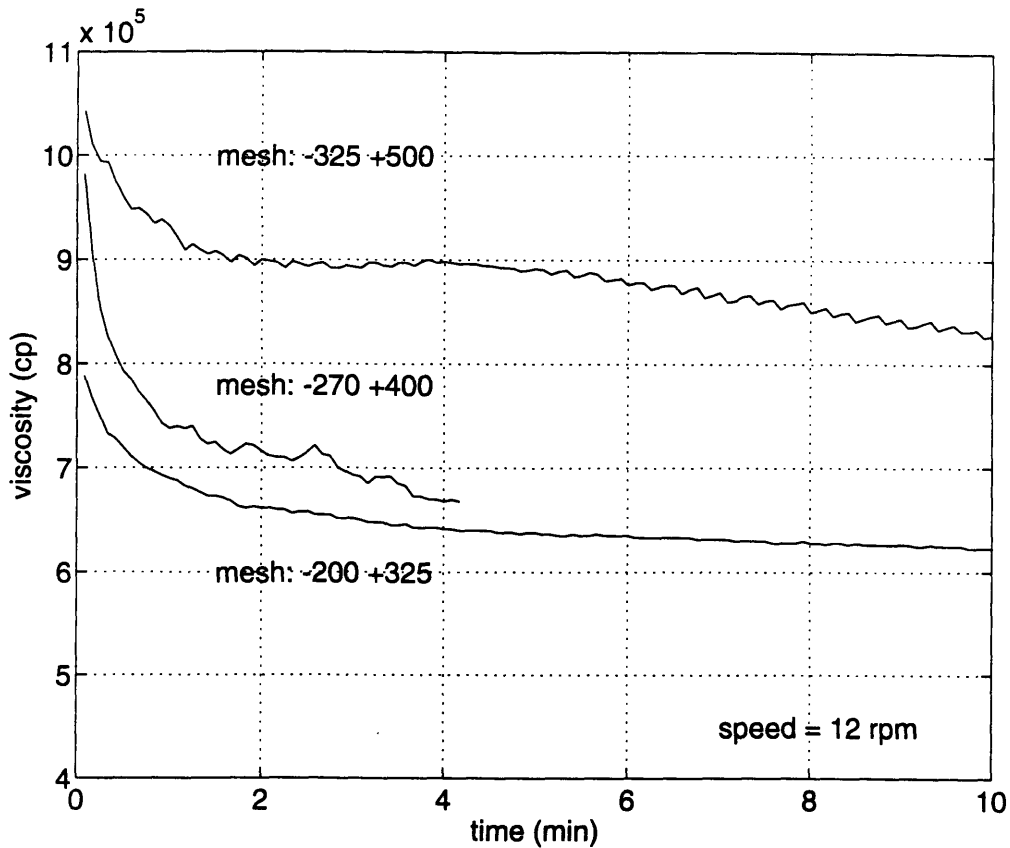
Figure 2-2: Viscosity decreases with time for a given rate of shear.

with time, as shown in Figure 2-2.

Thixotropic fluids generally reach an equilibrium viscosity $\mu_\infty$, which is attributed to the equalization of fluid breakdown with reformation and the alignment of fluid particles from an initial random state to a final state aligned with the direction of flow [22]. As a time dependent description, thixotropy characterizes the dynamic behavior of the fluid. If we consider a shear rate as a step input to the fluid, a certain amount of time is required for the apparent viscosity to reach its steady state value, at which point the fluid particles are aligned with the direction of flow. Further time dependent characteristics include stress relaxation, a phenomenon associated with the elastic properties of the fluid and is most relevant in characterizing the slumping properties of the paste.

Since our purpose is to deposit solder paste precisely by controlling process parameters, such as hydrodynamic pressure and flow rate, determination of the paste's mechanical properties as a function of shear rate, time, temperature, and humidity is not our primary goal. Rather, mechanical properties should be estimated directly

16

from measurements so that the printing equipment can either automatically compensate for variations by modulating printing parameters, such as squeegee speed and angle, or simply notify an operator of the material property drifts. The non-Newtonian thixotropic behavior makes a closed form analytical solution impossible for the squeegee/stencil geometry; however, model based closed loop control should be able to cope with the nonlinear dynamic behavior of the fluid.

Although closed loop control can deal with nonlinear time variant properties of the paste, the nature of the process imposes certain limitations. One limiting factor in paste deposition is the size of the solder particles. Pad dimensions of new SMDs are approaching the characteristic size of the particles, which limits, to an extent, the ability to deposit a consistent amount of paste at the desired thickness and uniformity. This is of concern, since the underlying assumption in all fluid solutions in that the fluid can be treated as a continuum. For macroscopic motion, like squeegee motion and corner flows, this is not an issue, but question remains as to what extent flow into the stencil apertures can be treated as motion of continuous fluid. For printing, the macroscopic phenomena are approaching the microscopic description of the fluid. One solution might consider decreasing the size of the paste particles. However, decreased particle size increases the surface area to volume ratio, which causes more oxidation per unit volume of paste, degrading solderability properties. To make the problem tractable, these microscopic effects have not yet been considered, although this type of flow phenomenon will be explored in future work.

# Chapter 3

# Fluid Mechanics of Printing and Corner Flows

The flow of solder paste into stencil apertures is induced by the hydrodynamic pressure developed at the squeegee tip by virtue of the squeegee motion. This pressure is the driving force for pumping the paste into stencil apertures. Not only will paste motion be affected by the tip pressure, but will also be a function of the paste viscosity, stencil wall roughness, aperture dimension, orientation, and operating conditions. Note that the stencil pattern is *a priori* information and nominal wall roughness is dictated by the manufacturing method. These issues, however, pertain to the *microflow* of paste into the stencil apertures. It is essential to first determine how squeegee motion induces a hydrodynamic pressure and how the height of the paste is related to this pressure and other machine variables. Ultimately, if fluid pressure at the squeegee tip can be controlled, the paste flowrate into the apertures, hence the height and uniformity of deposits, can be controlled. Furthermore since paste properties vary with machine inputs, environmental factors, and time, they must be estimated on-line to achieve superior process control.

## 3.1 Equations for Stokes' Flow

Despite data obtained from the Brookfield viscometer in Figure 2-1, for simplicity, the first assumption in deriving a model for the flow generated by the squeegee motion is that solder paste is Newtonian, i.e. $\mu = constant$. Considering this, and using the fact that the paste is an incompressible fluid,

$$\nabla \cdot \mathbf{v} = 0 \tag{3.1}$$

a momentum balance on the moving fluid yields the well known Navier-Stokes equation,

$$\rho \left( \frac{\partial \mathbf{v}}{\partial t} + \mathbf{v} \cdot \nabla \mathbf{v} \right) = -\nabla p + \mu \nabla^2 \mathbf{v} + \rho \mathbf{G} \tag{3.2}$$

For the squeegee/stencil geometry it is convenient to define a cylindrical coordinate system, as shown on Figure 3-1, in which case the $\nabla$ operator becomes,

$$\nabla = \left( \frac{\partial}{\partial r} \mathbf{r} + \frac{1}{r} \frac{\partial}{\partial \theta} \boldsymbol{\theta} + \frac{\partial}{\partial z} \mathbf{z} \right) \tag{3.3}$$

Assuming steady state plane polar flow, and ignoring the body forces $\rho \mathbf{G}$, the 2D fluid equations of motion in the $\mathbf{r}$ and $\boldsymbol{\theta}$ directions become,

$$\rho \left( v_r \frac{\partial v_r}{\partial r} + \frac{v_\theta}{r} \frac{\partial v_r}{\partial \theta} - \frac{v_\theta^2}{r} \right) =$$
$$-\frac{\partial p}{\partial r} + \mu \left[ \frac{\partial^2 v_r}{\partial r^2} + \frac{1}{r} \left( \frac{\partial v_r}{\partial r} \right) + \frac{1}{r^2} \left( \frac{\partial^2 v_r}{\partial \theta^2} \right) - \frac{v_r}{r^2} - \frac{2}{r^2} \left( \frac{\partial v_\theta}{\partial \theta} \right) \right] \tag{3.4}$$

$$\rho \left( v_r \frac{\partial v_\theta}{\partial r} + \frac{v_\theta}{r} \frac{\partial v_\theta}{\partial \theta} + \frac{v_\theta v_r}{r} \right) =$$
$$-\frac{1}{r} \frac{\partial p}{\partial \theta} + \mu \left[ \frac{\partial^2 v_\theta}{\partial r^2} + \frac{1}{r} \left( \frac{\partial v_\theta}{\partial r} \right) + \frac{1}{r^2} \left( \frac{\partial^2 v_r}{\partial \theta^2} \right) - \frac{v_\theta}{r^2} + \frac{2}{r^2} \left( \frac{\partial v_r}{\partial \theta} \right) \right] \tag{3.5}$$

The general solution to Equations 3.4 and 3.5 cannot be easily obtained unless certain terms in the equations can be neglected. Since fluid viscosity will be of the same order as squeegee speed, $O(1\frac{cm}{s})$, we will assume that inertial effects, $\mathbf{v} \cdot \nabla \mathbf{v}$, will be negligible compared to the viscous effects, $\mu \nabla^2 \mathbf{v}$. For this case, all of the terms on
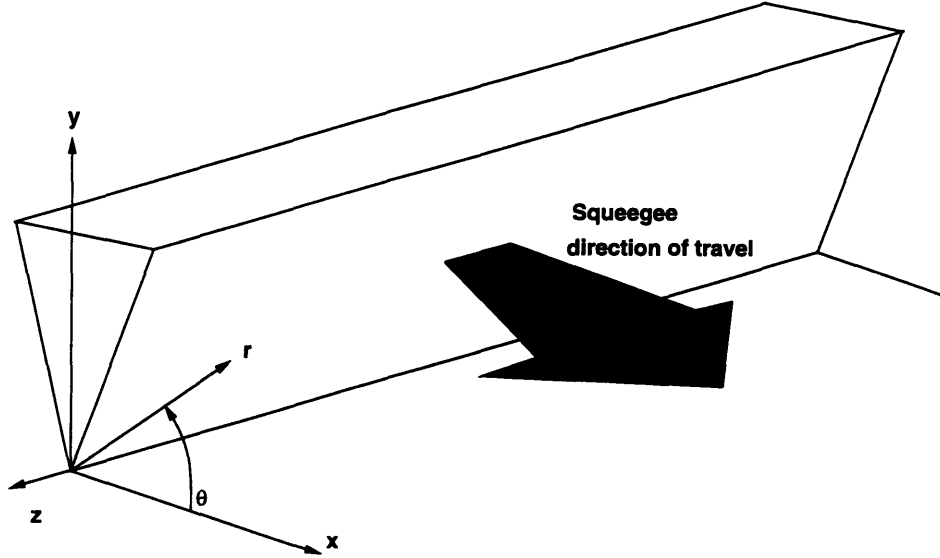
Figure 3-1: Cylindrical and cartesian coordinate axes

the left hand side of Equations 3.4 and 3.5 will be zero.

$$-\frac{\partial p}{\partial r} + \mu \left[ \frac{\partial^2 v_r}{\partial r^2} + \frac{1}{r}\left(\frac{\partial v_r}{\partial r}\right) + \frac{1}{r^2}\left(\frac{\partial^2 v_r}{\partial \theta^2}\right) - \frac{v_r}{r^2} - \frac{2}{r^2}\left(\frac{\partial v_\theta}{\partial \theta}\right) \right] = 0 \qquad (3.6)$$

$$-\frac{1}{r}\frac{\partial p}{\partial \theta} + \mu \left[ \frac{\partial^2 v_\theta}{\partial r^2} + \frac{1}{r}\left(\frac{\partial v_\theta}{\partial r}\right) + \frac{1}{r^2}\left(\frac{\partial^2 v_r}{\partial \theta^2}\right) - \frac{v_\theta}{r^2} + \frac{2}{r^2}\left(\frac{\partial v_r}{\partial \theta}\right) \right] = 0 \qquad (3.7)$$

By introducing the stream function $\psi = \psi(r, \theta)$ such that,

$$v_r = -\frac{1}{r}\frac{\partial \psi}{\partial \theta} \qquad (3.8)$$

$$v_\theta = \frac{\partial \psi}{\partial r} \qquad (3.9)$$

mass continuity of Equation 3.1 is automatically satisfied. Substituting Equation 3.8 and 3.9 into Equations 3.6 and 3.7, differentiating with respect to $r$ and $\theta$ respectively and summing the two equations to eliminate the pressure term, the general equation for steady incompressible *creeping* flow [23], often called Stokes' flow, can expressed

20

as a single equation given by

$$\nabla^4 \psi(r, \theta) = 0 \qquad (3.10)$$

This equation is called the *biharmonic equation* and often appears in elasticity theory. The goal is to find a solution to this $4^{th}$ order partial differential equation which satisfies the boundary conditions imposed by the squeegee/stencil geometry. The following list summarizes the assumptions in obtaining the biharmonic equation.

1. *The fluid in Newtonian.*

2. *Inertial effects are ignored, viscous effects dominate.*

3. *Flow is contained in the plane defined by $r$ and $\theta$.*

4. *The flow is in steady state.*

5. *Body forces are neglected.*

### 3.1.1   Corner Flow Solution

By the method of separation of variables [24], a solution to the biharmonic equation can be written as

$$\psi = r^\lambda f_\lambda(\theta) \qquad (3.11)$$

where $\lambda$ is any real or complex number and $r$ is the distance from the corner of the squeegee and stencil. For the viscous creeping solution to be valid the ratio of the inertial effects, $\rho \mathbf{v} \cdot \nabla \mathbf{v}$ to viscous effects, $\mu \nabla^2 \mathbf{v}$ in Equation 3.2 should be much smaller than unity. From the separated solution (Equation 3.11), [25] argued that the inertial term is negligible provided

$$R = \frac{A r^{p+1}}{\nu} \ll 1 \qquad (3.12)$$

where $R$ is the Reynolds number, $A$ is a nondimensional constant, $p$ is $\Re(\lambda - 1)$, and $\nu$ is the kinematic viscosity $\nu = \mu/\rho$. For $\Re(\lambda) < 1$, the velocity is unbounded at $r = 0$, hence the inertial forces cannot be ignored as the fluid tends towards the

21

origin. But for $\Re(\lambda) > 1$, inertial forces are negligible as $r$ approaches zero. (For a discussion of the effects of inertia at a corner, see [26].) For the problem of corner flow when a nonzero velocity is prescribed on one of the bounding surfaces, [9] used $\lambda = 1$ (Newtonian case). This solution is applicable to the corner flow of solder paste as the squeegee moves along the stencil. The stream function, $\psi(r, \theta)$, for Stokes' flow in a corner is given by,

$$\psi(r, \theta) = rU(B \sin \theta + C\theta \cos \theta + D\theta \sin \theta) \tag{3.13}$$

where $U$ is the speed of the scraping surface, in our case denoted by $V_{sq}$. The nonhomogeneous boundary conditions are

$$\psi = 0, \quad \tfrac{1}{r}\tfrac{\partial \psi}{\partial \theta} = U \quad \text{at} \theta = 0$$
$$\psi = 0, \quad \tfrac{\partial \psi}{\partial \theta} = 0 \quad \text{at} \theta = \alpha \tag{3.14}$$

where $\alpha$ is the angle of inclination of the squeegee with the horizontal plane. The $\psi(r, \theta) = 0$ conditions state that the there is no fluid flow relative to the bounding surfaces at the bounding surfaces; and that the no-slip condition states that the fluid velocity is zero at the squeegee surface, and $-U$ at the horizontal plane. With these conditions, the constants $B, C$, and $D$ are given by

$$B = \frac{-\alpha^2}{\alpha^2 - \sin^2 \alpha}, \ C = \frac{\sin^2 \alpha}{\alpha^2 - \sin^2 \alpha}, \ D = \frac{\alpha - \sin \alpha \cos \alpha}{\alpha^2 - \sin^2 \alpha} \tag{3.15}$$

Figure 3-2 and 3-3 show the streamlines for squeegee angles $\alpha$ of $\frac{\pi}{4}$ and $\frac{\pi}{6}$.

## 3.1.2 Velocities, Strain Rates, and Stresses

The streamline function is significant because velocity, strain rate, and stress distributions can be determined directly by substitution into the equations of motion. Furthermore, the stresses can be integrated to give the forces acting on the squeegee face, which is significant since these forces can be the primary measurements used for real-time process monitoring. When included into a model which accounts for friction
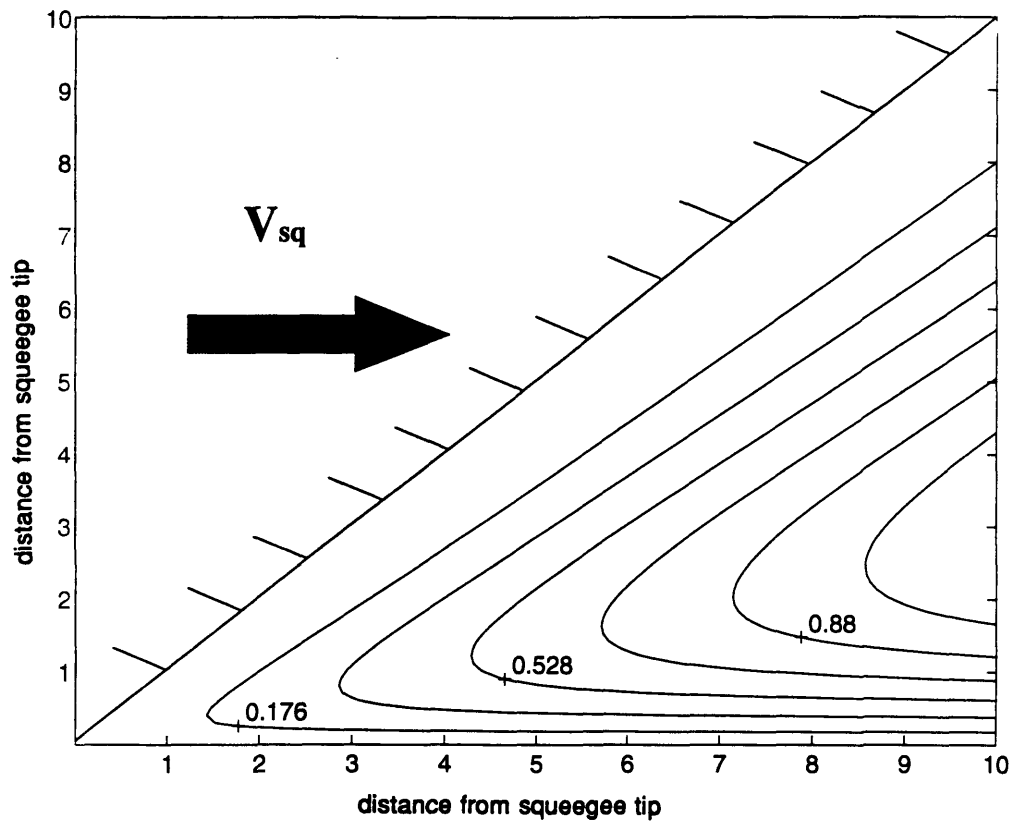
22

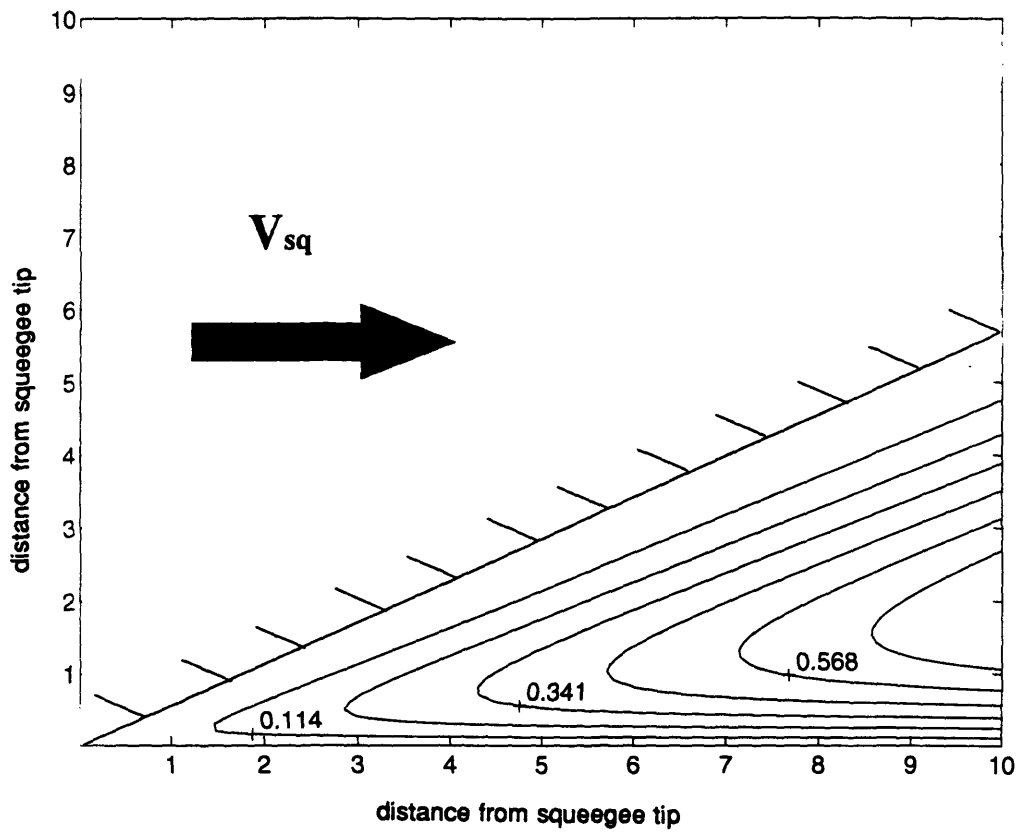Figure 3-2: Streamline plot for Taylor's solution for $\alpha = \frac{\pi}{4}$.

Figure 3-3: Streamline plot for Taylor's solution for $\alpha = \frac{\pi}{6}$.

and contact forces, the *in-situ* force measurements can be exploited to describe the hydrodynamics of the paste motion and provide information relevant to the current state of the solder paste.

The radial and theta components of the velocity are readily calculated using Equations 3.8 and 3.9,

$$
\begin{aligned}
v_r &= -V_{sq}\left(B\cos\theta + C(\cos\theta - \theta\sin\theta) + D(\sin\theta + \theta\cos\theta)\right) \\
v_\theta &= V_{sq}\left(B\sin\theta + C\theta\cos\theta + D\theta\sin\theta\right)
\end{aligned}
\tag{3.16}
$$

The magnitude of the rate of strain, $\dot\gamma$, is calculated from the second invariant of the strain rate tensor by the relation,

$$
\dot\gamma = \sqrt{\frac{1}{2}\mathbf{II}_{\dot\gamma}}
\tag{3.17}
$$

where $\mathbf{II}_{\dot\gamma} = tr\dot\gamma^2$. For the case of plane polar shear flow, the second invariant of the strain rate tensor is simply,

$$
\mathbf{II}_{\dot\gamma} = \dot\gamma_{r\theta}^2\, tr\begin{pmatrix} 1 & 0 & 0 \\ 0 & 1 & 0 \\ 0 & 0 & 0 \end{pmatrix} = 2\dot\gamma_{r\theta}^2
\tag{3.18}
$$

Therefore, the magnitude of the rate of strain is simply the $r,\theta$ shear component of the tensor, as to be expected in this type of flow. In plane polar coordinates the shear rate is given by,

$$
\dot\gamma_{r\theta} = \dot\gamma_{\theta r} = r\frac{\partial}{\partial r}\left(\frac{v_\theta}{r}\right) + \frac{1}{r}\frac{\partial v_r}{\partial\theta}
\tag{3.19}
$$

By direct substitution of Equation 3.16 into Equation 3.19, the shear rate for the forced corner flow is obtained and given by,

$$
\dot\gamma_{r\theta} = \frac{2V_{sq}}{r}\left(C\sin\theta - D\cos\theta\right)
\tag{3.20}
$$

25

Since we are dealing with a Newtonian fluid, the shear stress, $\tau$, is given by,

$$\tau_{r\theta} = \mu \dot{\gamma}_{r\theta} = \mu \frac{2V_{sq}}{r} \left( C \sin\theta - D \cos\theta \right) \tag{3.21}$$

The pressure distribution is obtained by substitution and integration of the velocities of Equation 3.16, into Equation 3.6 and Equation 3.7, given by the relationship,

$$p_r = p_\theta = \frac{2\mu V_{sq}}{r} \left( D \sin\theta + C \cos\theta \right) \tag{3.22}$$

Contours of constant stress and shear are shown in Figures 3-4 and 3-5 for squeegee angles of $\alpha = \frac{\pi}{4}$ and $\frac{\pi}{6}$. The broken line represents contours of constant pressure, while the solid line represents contours of constant shear. This data was generated using unity values for squeegee velocity and viscosity. Note that when using a value of 1 Pa s for viscosity, the shear and shear rate are identical.

Another study of the shear rates induced during rolling motion was conducted by [12], but in the analysis, it was assumed that the fluid motion was only one dimensional. For distances along the bounding surfaces and distant from the corner, numerical values for the shear rates are reasonably close to the exact values calculated from Equation 3.20 and shown in Figure 3-4. However, at the squeegee/stencil interface, where the shear rate approaches the singularity and curvature effects dominate the flow pattern, results from [12] are incorrect.

As a similarity solution, the above analysis assumed an infinite amount of fluid in front of the squeegee. An investigation of a finite amount of paste has been conducted by [11]. In this study, the free surface of the rolling paste and a more complex geometry was used, which included the bounding surface of the squeegee holder. With the introduction of these complexities, the solution to the Navier-Stokes equations was calculated numerically. Interestingly, despite the additional boundary conditions and the free surface of the paste, numerical values of the shear rate and pressure are in close agreement with the values obtained by Equations 3.21 and 3.22. To an extent, this was to be expected, since Equations 3.21 and 3.22 show that the stresses decrease as $\frac{1}{r}$ from the squeegee tip, and occurances far from the origin have neglegible effect.
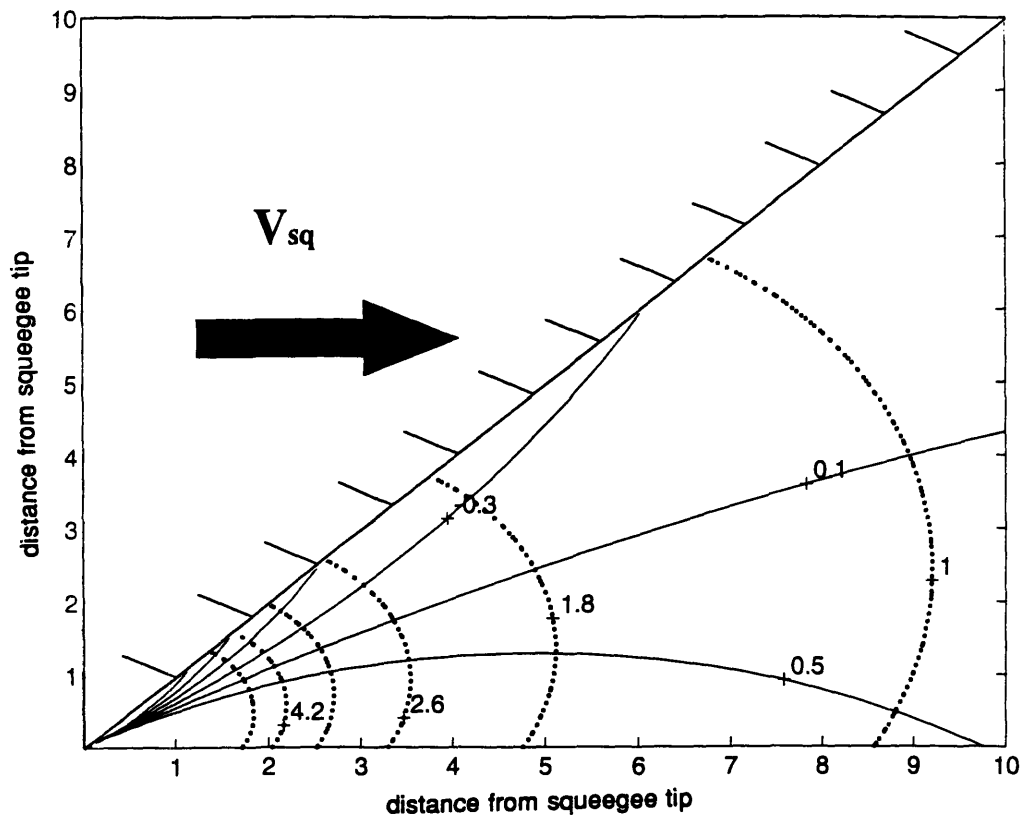
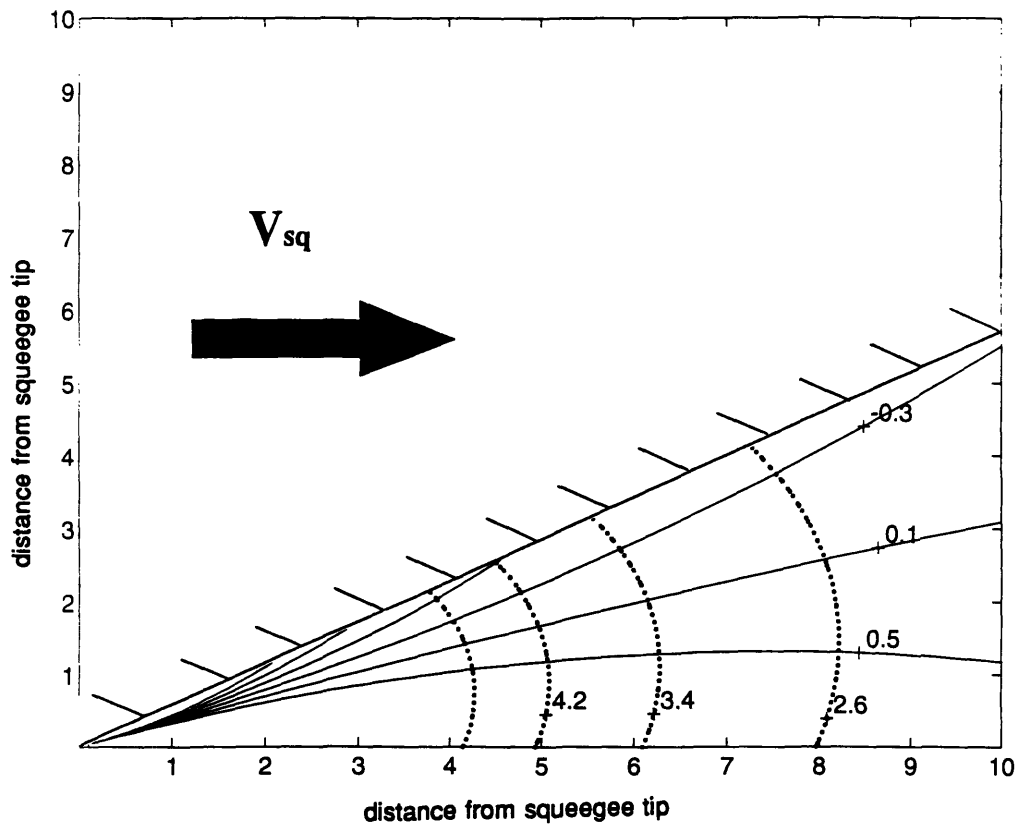Figure 3-4: Lines of constant shear and pressure for an angle of $\frac{\pi}{4}$

Figure 3-5: Lines of constant shear and pressure for an angle of $\frac{\pi}{6}$

This suggests that the volume of paste in front of the squeegee has little effect on the hydrodynamic pressures.

## 3.2   A Note About Printing Control

Ultimately, the height of the printed deposit is of interest. Paste height can be controlled by modulating machine settings in accordance with changes in the fluid characteristics. It is of interest to determine the sensitivity of hydrodynamic pressure to changes in control signals.

[13] and [14] applied a continuity equation in time to a volume of paste being deposited into the substrate. In their analysis, it was shown that the height of the paste, $h_p$, is related to the height of the stencil, $h_{st}$ by the relation,

$$h_p = h_{st} \left( 1 + \frac{V_p}{V_{sq}} \right) \tag{3.23}$$

where $V_p$ is the velocity of the paste underneath the squeegee and $V_{sq}$ is the squeegee speed, as usual. This relationship suggests that controlling the pressure by modulating the squeegee velocity alone may be insufficient, if $V_p$ is a linear function of $V_{sq}$. However, the pressure can also be controlled by changing the squeegee angle. An analysis of the sensitivities of pressure to angle and squeegee speed will demonstrate the importance of dynamic control of the squeegee angle.

By inspection of Equation 3.21 and Equation 3.22, the changes in the stresses with respect to changes in squeegee speed are given by,

$$\Delta p_r = \frac{2\mu V_{sq}}{r} \left( \frac{\alpha \sin \alpha}{\alpha^2 - \sin^2 \alpha} \right) \Delta V_{sq} \tag{3.24}$$

$$\Delta \tau_{r\theta} = \frac{2\mu V_{sq}}{r} \left( \frac{\sin \alpha - \alpha \cos \alpha}{\alpha^2 - \sin^2 \alpha} \right) \Delta V_{sq} \tag{3.25}$$

Numerically, the result is that an incremental change in the squeegee speed causes the same incremental change in the fluid stresses. However, this is not necessarily true for the squeegee angle $\alpha$, due to the nonlinear dependence. By evaluating the

expressions for pressure and shear at the squeegee and differentiating with respect to $\alpha$, the following relationships are established for the sensitvities,

$$\Delta p_r = \frac{\partial p_r}{\partial \alpha}\Delta\alpha$$

$$= \frac{2\mu V_{sq}}{r}\left(\frac{\sin\alpha + \alpha\cos\alpha}{\alpha^2 - \sin^2\alpha} - \frac{(2\alpha\sin\alpha)(\alpha - \cos\alpha\sin\alpha)}{(\alpha^2 - \sin^2\alpha)^2}\right)\Delta\alpha \qquad (3.26)$$

$$\Delta\tau_{r\theta} = \frac{\partial\tau_{r\theta}}{\partial\alpha}\Delta\alpha$$

$$= \frac{2\mu V_{sq}}{r}\left(\frac{\alpha\sin\alpha}{\alpha^2 - \sin^2\alpha} - \frac{2(\sin\alpha - \alpha\cos\alpha)(\alpha - \cos\alpha\sin\alpha)}{(\alpha^2 - \sin^2\alpha)^2}\right)\Delta\alpha \qquad (3.27)$$

Evaluating Equations 3.26 and 3.27 for a 10% decrease in squeegee angle from 45° to 40.5° gives a a 20% increase in stress and 14% increase in shear. These results illustrate the utility of dynamic angle control. Fluid stresses can be controlled without changing squeegee velocity, however pressure control by angle actuation may be difficut since these stresses are nonlinear with $\alpha$.

## 3.3 Extension to Generalized Newtonian Corner Flow

Recent research in the area of forced corner flows for non-Newtonian fluids has concentrated on applications for polymer processing, where secondary flows and instabilities due to stationary corners are caused in the viscoelactic fluids [27]. These flow situations arise when fluid encounters a constriction in a pipe or exits into a reservoir or other transport mechanisms [28], [29]. The solutions for these types of corner flows are numerical and satisfy homogeneous boundary conditions, unlike the squeegee/stencil geometry, in which nonhomogeneous boundary conditions are prescribed. Nonetheless, the technique for solving generalized Newtonian corner flow for both situations is identical and is of academic interest.

The key idea in solving the corner flow problem for non-Newtonian fluids is the assumption that the streamline function can be expressed as a separated series expansion given by,

$$\psi(r,\theta) = \sum_{k=1}^{\infty} \Re\left(A_k r^{\lambda_k} f_k(\theta)\right) \qquad (3.28)$$

where

$$\lambda_0 < \Re(\lambda_1) < \Re(\lambda_2) \cdots \qquad (3.29)$$

As $r$ approaches the origin, only the term associated with the first eigenvalue will appear in the solution. By differentiating Equation 3.28 to obtain the velocities, the strin rate tensor can be calculated by $\dot{\gamma} = \nabla v + \nabla v^{\dagger}$, where $\nabla v^{\dagger}$ is the transpose of the dyadic $\nabla v$.

The stresses can then be computed using a power law relation. Using this result, [30] obtained a $4^{th}$ order ordinary differential equation for $f(\theta)$. Solutions for the streamline function were calculated numerically using a shooting method for flow about a stationary corner. Numerical solution to corner flows with nonhomogeneous boundary conditions was considered by [31], but could not be found due to numerical instabilities. Currently, numerical solution to the corner flow problem of a power law fluid with nonhomogeneous boundary conditions is being investigated. Hopefully, the numerical instabilities encountered by [31] can be overcome.

# Chapter 4

# Squeegee Modeling and Experimental Verification

Up to this point, we have concentrated our attention to the development of a solution for the stress distribution generated within the solder paste during printing. Since obtaining a closed form analytical solution for the streamline function was impossible for non-Newtonian corner flows, the problem was simplified by assuming Newtonian flow. For this particular case, the streamline function for corner flow with nonhomogeneous boundary conditions was determined by [10].

Although fluid solutions of this sort alone are intriguing, they must be incorporated into a more comprehensive model of the printing process if real time process estimation and control is to be achieved. This chapter extends the discussion of the mechanics of solder paste flow, and applies the results obtained in Chapter 3 to a model containing additional forces acting on the squeegee during printing. By including friction and contact forces, the connection is made between the fluid dynamics of corner flow and *in-situ* measurements for process monitoring. Experimental results are contained within this chapter and are compared to the analytically derived linear model. A nonlinear empirical model relating machine paramters, measurements, and process variables is then proposed.

# 4.1 Squeegee forces

The previous chapter used the streamline function developed by Taylor to obtain the shear and normal stresses in the fluid as a function of fluid viscosity $\mu$, squeegee velocity $V_{sq}$, and angle of inclination $\alpha$. By evaluating the stresses along the squeegee face, the stresses can be resolved in convenient directions, and integrated to yield the forces which are generated by the paste motion. The stresses per unit length of squeegee in the $r$ and $\theta$ directions given by Equations 3.21 and 3.22 can easily be evaluated along the squeegee by letting $\theta = \alpha$. For convenience, these stresses are resolved in the $x$ and $y$ directions as defined in Figure 3-1,

$$P_x = \frac{2\mu V_{sq}}{r}\left(\frac{\sin^2\alpha}{\alpha^2 - \sin^2\alpha}\right) \tag{4.1}$$

$$P_y = \frac{2\mu V_{sq}}{r}\left(\frac{\alpha - \sin\alpha\cos\alpha}{\alpha^2 - \sin^2\alpha}\right) \tag{4.2}$$

To obtain the fluid forces acting on the squeegee, these pressures must be integrated over the area of fluid contact. Unfortunately, the singularity at the origin causes the forces to become unbounded. However, a more realistic model recognizes that the dimension of the corner at the squeegee/stencil interface will never be zero, but rather will be a characteristic size of any edge defects or thickness of a lubrication film as shown in Figure 4-1. The lubricating film consists of flux binder, while the bulk flow of paste particles and its constituents are still governed by the Taylor solution. This notion of lubrication does not disturb the fluid pattern calculated by the streamline function, but rather is used as a conceptual tool to avoid the unrealistic case of infinite fluid forces at the origin. The fluid pressures of Equation 4.1 and 4.2, can be integrated from this characteristic length, denoted by $a$, to the point where the solder paste separates and rolls, distance L, to yield the hydrodynamic forces per unit length in the $x$ and $y$ directions,

$$
\begin{aligned}
F_{hyd_x} &= \int_a^L P_x dr \\
&= 2\mu V_{sq}\left(\frac{\sin^2\alpha}{\alpha^2 - \sin^2\alpha}\right)\ln\left(\frac{L}{a}\right)
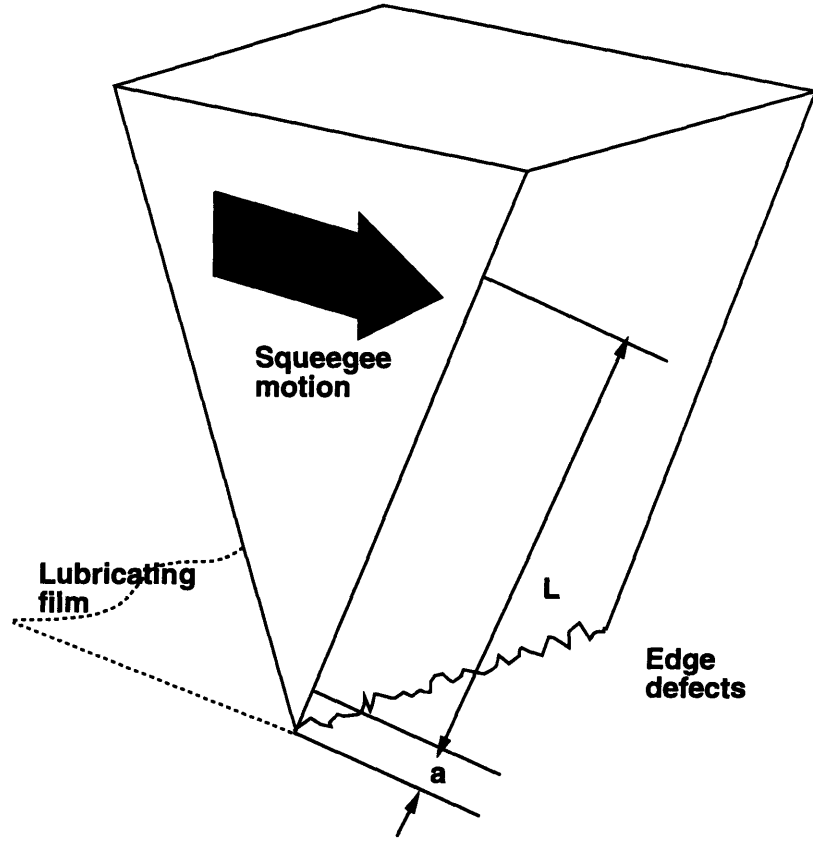\end{aligned} \tag{4.3}
$$

Figure 4-1: Thin film lubrication during printing.

$$F_{hyd_y} = \int_a^L P_y dr$$

$$= 2\mu V_{sq} \left( \frac{\alpha - \sin\alpha\cos\alpha}{\alpha^2 - \sin^2\alpha} \right) \ln\left( \frac{L}{a} \right) \tag{4.4}$$

The term $\ln\left(\frac{L}{a}\right)$ which resulted from the integration is significant because it suggests that the volume of paste has negligible effect of the forces generated by the paste motion. By considering $F_{hyd} \propto \ln\left(\frac{L}{a}\right)$, the change in force due to a change the the volume of paste can be written as,

$$\Delta F(L/a) = \frac{\partial F}{\partial(L/a)} \Delta\left(\frac{L}{a}\right) = \frac{a}{L}\Delta\left(\frac{L}{a}\right) \tag{4.5}$$

Since $a$ is a characteristic size of the lubricating flux or squeegee edge defects, $O(\mu m)$, the ratio $\frac{a}{L} \ll 1$. The negligible effect of volume on generation of the fluid forces is in agreement with the numerical results obtained by [11]. The consequence of this result is that the fluid properties can be estimated on-line without precise knowledge of solder volume.
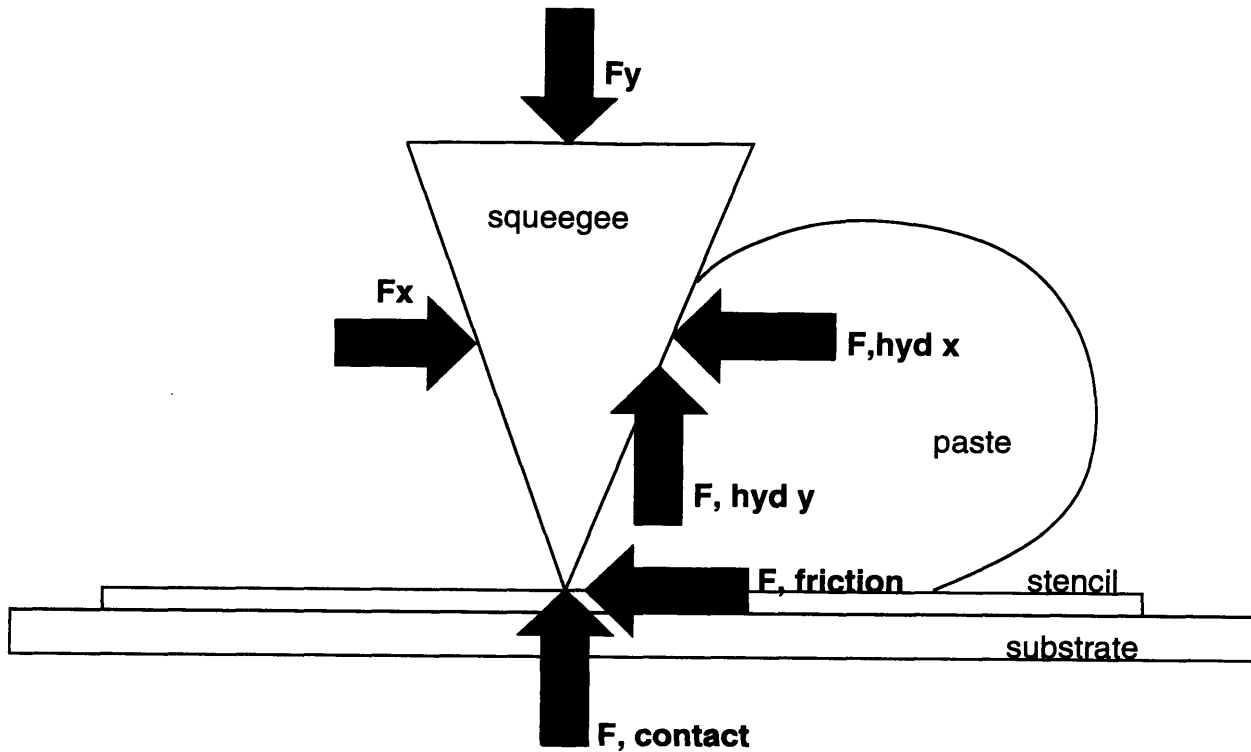
Figure 4-2: Forces acting on the squeegee during printing

Other work in evaluating the pressures and forces induced during printing has been conducted by [13], [14], and [15]. [13] included non-Newtonian behavior in their analysis, but their solutions were too complex for use in any control or estimation scheme. Their equations rely on parameters which can neither be measured directly nor estimated indirectly, and any solution for pressures, velocities, or deformation is an iterative procedure. Huner's discussion [15] of the pressure forces was based on the equations pertinent to lubrication theory. In that analysis, single dimensional Navier-Stokes equations were used. Because of this, his analysis is only valid for a Newtonian fluid flowing beneath a squeegee with extremely small angles. His analysis is inappropriate for describing the rolling motion of the paste. The Taylor solution remains the most suitable solution for describing the fluid flow at the squeegee/stencil interface.

The hydrodynamic forces, however, are not the only forces which act on the squeegee during printing. Additional expressions for friction and contact must be included in the model. These forces are illustrated in Figure 4-2. A simple force

balance for this system establishes the following relationships,

$$F_x = F_{friction} + F_{hyd_x} \qquad (4.6)$$

$$F_y = F_{contact} + F_{hyd_y} \qquad (4.7)$$

where $F_{hyd_x}$ and $F_{hyd_y}$ are given by Equations 4.3 and 4.4 and the frictional force is modeled as

$$F_{friction} = \eta F_{contact} \qquad (4.8)$$

Solving for $F_{contact}$ in Equation 4.7, substituting into Equation 4.8 and rearranging terms, the following expression is obtained for the total force acting on the $x$ direction opposing squeegee motion,

$$F_x = \eta \left( F_y - F_{hyd_y} \right) + F_{hyd_x} \qquad (4.9)$$

By grouping terms and using the previously derived expressions for the hydrodynamic forces, $F_x$ can be written as

$$F_x = a_1 V_{sq} f_1(\alpha) + a_2 V_{sq} f_2(\alpha) + a_3 F_y \qquad (4.10)$$

where $a_1 = 2\mu \ln \left( \frac{L}{a} \right)$, $a_2 = -2\eta\mu \ln \left( \frac{L}{a} \right)$, $a_3 = \eta$, and $f_1(\alpha)$ and $f_2(\alpha)$ are the nonlinear functions appearing in the equations for the hydrodynamic stresses. This result is useful since measurable quantities and machine inputs, such as angle of inclination, squeegee speed, and downward force, are linearly related by parameters which are relevant to the paste and squeegee/stencil properties. By measuring the forces acting on the squeegee in the $x$ and $y$ directions, estimation algorithms can be applied to determine the values of the parameters in Equation 4.10 in real time. The linearity is beneficial since parameter estimation techniques for linear systems have the desirable property of rapid convergence, making their implementation in an on-line environment ideal.

## 4.2 Hardware

It is evident that determination of the hydrodynamic pressures and estimation the fluid viscosity and friction coefficient requires measurement of squeegee forces. A two degree-of-freedom force sensor was constructed and placed on the squeegee assembly of an MPM SP200 semi-automatic paste printer for this purpose. Also, signals from a rotary potentiometer encoder were acquired to obtain the squeegee velocity. Due to hardware limitations, the squeegee angle was fixed at 45°. The print head assembly with the 2-dof load cell is as shown in Figure 4-3.

The print head assembly was driven by the ram at point (G) from compressed air on oil cylinders. Squeegee velocity was measured by the rotary potentiometer encoder at (H), while the $y$ direction force was measured by strain gauges at (C), and the $x$ direction force was measured by strain gauges at (B). The strain gauges at both locations were arranged in a full bridge pattern to eliminate temperature effects, and the signals were filtered and amplified using low noise, low bias current instrumentation amplifiers. Data was collected using a Dell 386 computer equipped with a National Instruments AT-MIO-16 data acquisition board. Additional circuitry included various relays and digital triggers to actuate the print cycle and to begin and end data collection automatically.

## 4.3 Model Verification

The first assumption that the fluid was Newtonian was tested by measuring the average $x$ component of force $F_x$, as a function of the squeegee velocity for an entire print cycle. Clearly, if the solder paste could be described as a Newtonian fluid, $F_x$ would be directly proportional to the squeegee speed, $V_{sq}$. That is, for all shear rates encountered in this type of flow, the constant of proportionality would be the viscosity of the fluid. The force/speed behavior is as shown in Figure 4-4. Each point in Figure 4-4 plot is the average force at a specified velocity for an entire print cycle.

37

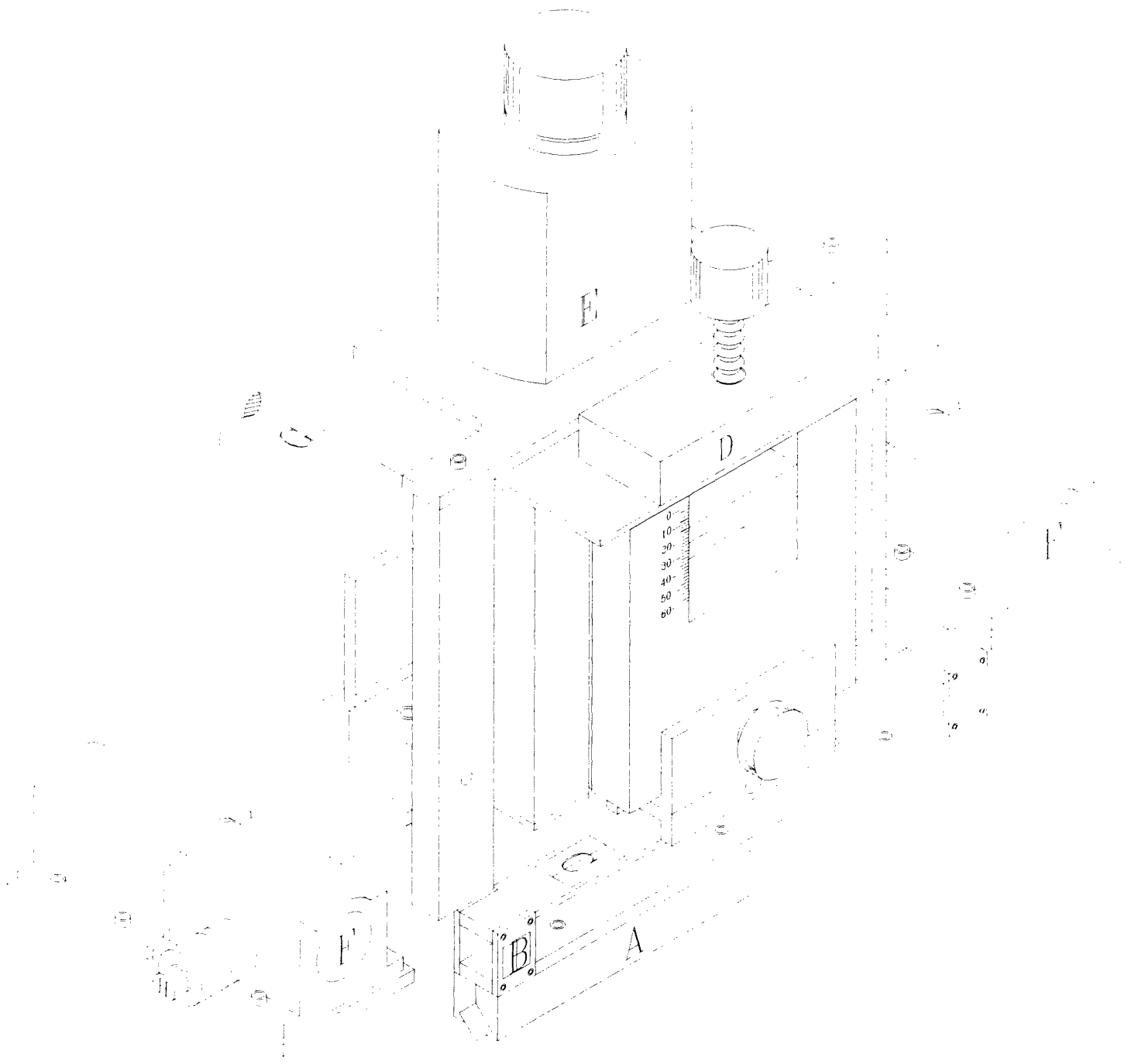Figure 4-3: MPM SP200 Print head assembly, equipped with a rotary potentiometer encoder to measure squeegee speed (H), and strain gauges at (B) and (C) to measure the $x$ and $y$ components of force.
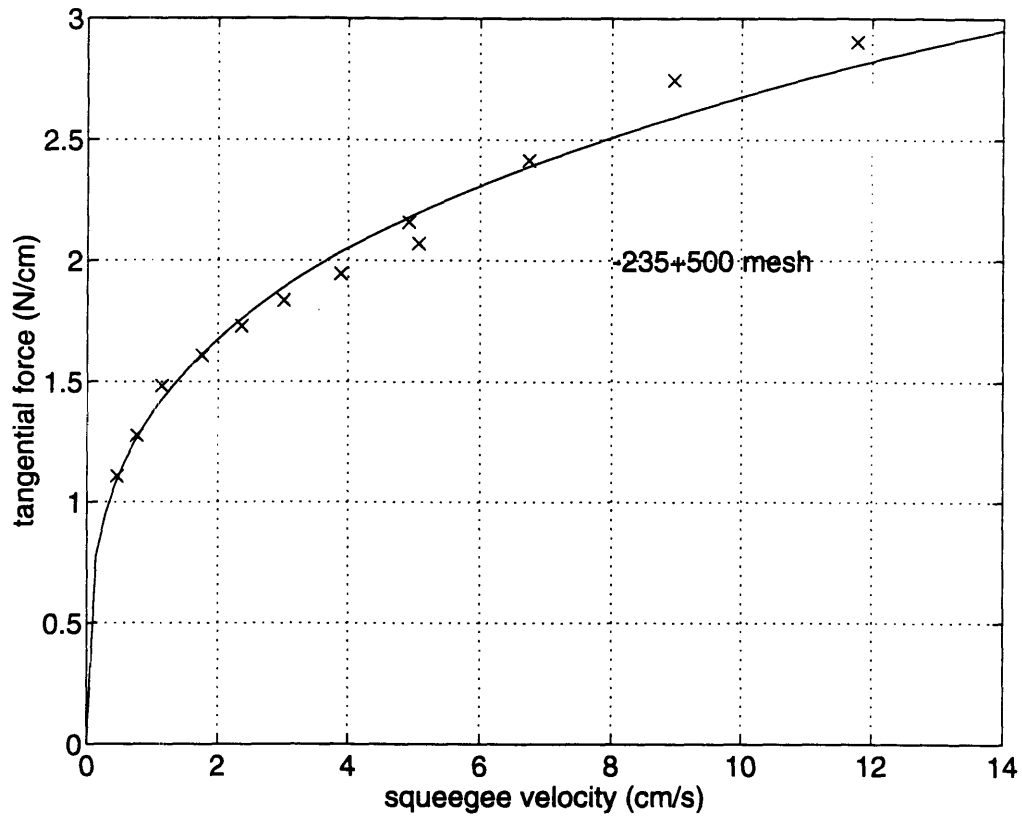
Figure 4-4: Measurements from the printing machine show the non-Newtonian characteristics of the solder paste. Note that the curve is approximately linear in the machine operating region (3 to 9 $\frac{cm}{s}$).

The most notable result is that the force/velocity behavior is not linear, but rather displays the same nonlinear behavior of shear rate for a power law fluid. This is to be expected, as shear rates in the paste are smaller for low squeegee velocities than the rates at higher speeds. Since the force measurements are in essence capturing the integrated shear rates, the "viscosity" of the fluid at slower squeegee speeds is larger than the "viscosity" of the fluid at higher speeds. Furthermore, because it has been established that pressures dominate the measurements at the squeegee tip, the viscosity of the fluid within this region of highest shear rates are mostly reflected in the force measurements. The significant result is that although the viscosity is a function of the squeegee speed, the force/velocity behavior is relatively constant over the working range (3 to 9 $\frac{cm}{s}$) of most machines in production. This suggests that for the ranges of shear rates generated by the squeegee motion in this region, the fluid can be characterized by a constant of proportionality. For convenience, this constant is still called viscosity, but will be denoted by $\mu_f$ to emphasize that this number is a value corresponding to the viscosity of integrated shear rates for a particular squeegee speed. Note that even if the working range of squeegee speeds were to include regions with more pronounced nonlinear behavior, a piecewise linear approximation would still yield meaningful results.

An assumption in deriving expressions for the fluid forces was to integrate the pressures from a small distance away from the tip to avoid the singularity. The result of this indicated that the volume of paste has negligible influence on the fluid pressures. Data was gathered by removing a given quantity of paste for each print cycle. Initially, a paste bead with $L \approx 1cm$ was tested. For subsequent print cycles, the volume was decreased by approximately $\frac{1}{3}$. No noticeable change of the force measurements was observed. The benefit of this result is that the material properties can be estimated without *a priori* knowledge of the paste volume. However, this also indicates that a loss in material volume cannot be detected by the force measurements. Measurement of paste volume is an important criteria in the printing operation, since enough material must be present to properly print stencil patterns.

Another test measured the importance of the normal force $F_y$. For $F_y$ ranging

from 10 to 20 lbs, $F_x$ did not vary significantly, indicating that the friction force was negligible compared to the hydrodynamic force generated by squeegee motion. A constant squeegee speed was used for these tests to ensure that the fluid forces would not affect the results. The results were consistent with our assumption which avoided the singularity in obtaining the hydrodynamic forces by claiming that a thin film would lubricate the stencil, hence decreasing any friction considerably. This should not suggest that force measurements in the $y$ direction are unimportant, since this information is still required for closed loop control of squeegee downward force.

The force sensors had to be sensitive enough to detect changes of the paste properties due to shear thinning and solvent evaporation if on-line material monitoring was to be useful. The thixotropic behavior was observed during operation of the printing machine over a long duration as shown in Figure 4-5. Despite the noise of the force sensor readings, shear thinning was observed. Each line in Figure 4-5 represents one print cycle. For 20 prints, the measured $F_x$ decreased by approximately 15 percent. The initial negative force occurs when the squeegee is lowered to the surface of the stencil. The squeegee tip pivots in the direction opposite that of travel before printing. In that configuration, the force is compressive. When the squeegee assembly begins moving, the tip immediately pivots in the direction of motion, resulting in a positive tensile state. When the static friction is overcome and the entire squeegee tip begins to move with the assembly, the measured force is that force generated by friction and rolling motion of the paste. Average force values from Figure 4-5 versus print cycle are shown in Figure 4-6.

## 4.4 An Empirically Derived Nonlinear Model

Simple experiments demonstrated that many of the assumptions in obtaining the linear model for the fluid motion and squeegee forces were valid. The friction force was found to be negligible due to thin film lubrication, paste volume did not contribute to measured forces, and the force sensors had sufficient resolution to observe changes in paste viscosity over time. However, non-Newtonian behavior of the paste was observed
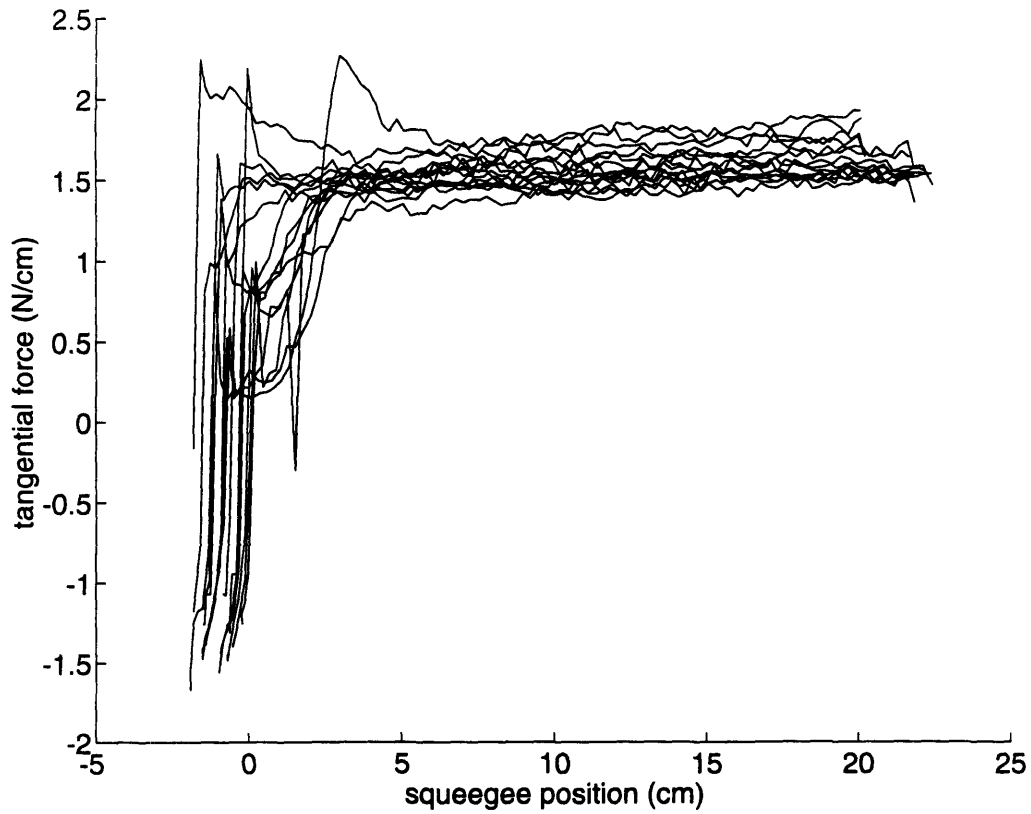
41

Figure 4-5: Each line represents a print cycle. Due to the thixotropic properties, the viscosity decreases towards a steady state value after approximately 20 cycles.
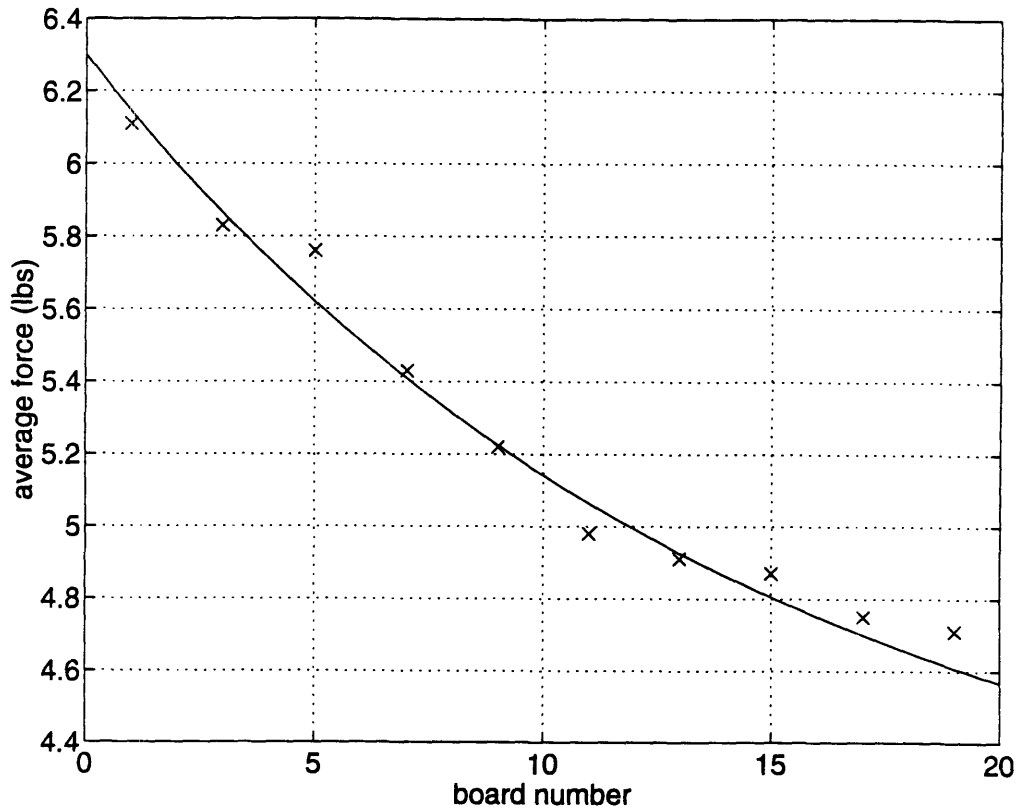


Figure 4-6: Average force values versus print cycle.

in the experiments which measured the force/velocity characteristics. Although the linear approximation is valid for small ranges of squeegee speed, a nonlinear power law model was derived based on empirical results.

The data shown in Figure 4-4 can be fitted with a curve of the form $F_x = kV_{sq}^n$. Assuming that the fluid forces generated by the squeegee motion can be described by a power law expression, the linear model given by Equation 4.10 can be modified and written in the form,

$$F_x = a_1' V_{sq}^n f_1(\alpha) + a_2' V_{sq}^n f_2(\alpha) + a_3' F_y \qquad (4.11)$$

The constants $a_i'$ are the same as the $a_i$ of the linear model, except that the viscosity $\mu$ is replaced by the constant $k$, which is representative of the thickness of the fluid. The nonlinear functions $f_1(\alpha)$ and $f_2(\alpha)$ remain the same since an empirical model of the angular dependence could not be evaluated due to hardware limitations.

The importance of both the linear and nonlinear models is that measurable signals are related to machine parameters and other quantities which have physical significance. When expressed is a linear form, standard parameter estimation schemes can be applied. This is the subject of Chapter 5.

# Chapter 5

# Estimation Technique for Process Monitoring

In Chapter 4, a linear model of the fluid, friction, and contact forces was derived from first principles and evaluated through a series of simple experiments. From these experiments, the linear approximation was shown to be valid over a small operating range of printing speeds. An empirically derived nonlinear model extended the analysis to include a more general decription of the squeegee force/speed behavior. In both cases, measureable quantities were related to machine settings and other parameters. On-line estimation of these parameters is critical, since they are related to solder paste properties and the squeegee/stencil interface. For the linear model, a recursive least squares algorithm was directly applied to obtain estimates, while for the nonlinear model, some algebraic manipulation was required to recast the equations in linear form so that the same algoithm could be implemented. In this chapter, the estimation techniques are described, and experimental results of the paramter estimation for the linear and nonlinear model are presented.

## 5.1   Additional Modeling

As previously mentioned, due to hardware limitations, the squeegee angle was fixed at 45°. Because of this, experimental results could not be obtained to verify the

expressions for $f_1(\alpha)$ and $f_2(\alpha)$. For constant squeegee angles, the models in Equation 4.11 and Equation 4.10 could further be rearranged. The linear model with constant squeegee angle can be rewritten as,

$$F_x = b_1 V_{sq} + b_2 F_y + b_3 \qquad (5.1)$$

where $b_1 = a_1 f_1(\alpha) + a_2 f_2(\alpha)$, $b_2 = a_3$, and $b_3$ is the intercept term of the line in the $F_x, V_{sq}$ plane. This intercept is a consequence of the nonlinear behavior of the solder paste. Notice that for a Newtonian fluid, $b_3 = 0$. Over an operating range where the linear approximation is valid, the nonzero intercept term could be interpreted as a yield point of the paste, while the slope of the line could be considered as the fluid viscosity. The yield point is the minimum value of the applied stress which causes the fluid to flow. Materials which exhibit this type of behavior are called *Bingham Plasitcs*. Since the relationship in Equation 5.1 is linear in its coefficients, and any significant variation in the parameters $b_{1,2,3}$ occur over a long time scale, standard parameter estimation techniques are appropriate for on-line estimation of material properties. With application of this technique, solder paste and tool properties can be estimated on-line and can track any variations to these parameters independently.

In order to apply the same estimation scheme to the nonlinear model, some mathematical manipulation is required. First, by grouping the $f_i(\alpha)$ terms, the nonlinear model of Equation 4.11 can be rewritten as,

$$F_x = b_1' V_{sq}^{b_2'} + b_3' F_y \qquad (5.2)$$

where $b_1' = a_1' f_1(\alpha) + a_2' f_2(\alpha)$, $b_2' = n$, and $b_3' = a_3'$. The first step of the estimation scheme is to estimate $b_3'$ for constant squeegee velocity. When the squeegee speed is constant, Equation 5.2, collapses to the form,

$$F_x = constant + b_3' F_y \qquad (5.3)$$

Convergence to the *constant* and $b_3'$ using the least squares algorithm is rapid, since

the algorithm only has to estimate one slope and one intercept. The friction term $b'_3$ is associated with tool wear and the interface between the squeegee and stencil. Because any variation to the friction coefficient will occur over a long time scale relative to the time associated with any paste changes, the $b'_3 F_y$ can be treated as a constant and moved to the left hand side of Equation 5.2 giving the following expression,

$$F_x - b'_3 F_y = b'_1 V_{sq}^{b'_2} \tag{5.4}$$

By taking the logorithm of both sides of Equation 5.4, the equation is recast into a form whereby the unknown coefficients are linearly invloved with measurable signals and machine settings.

$$\log(F_x - b'_3 F_y) = b'_2 \log(V_{sq}) + \log(b'_1) \tag{5.5}$$

In this form, the least squares estimation algorithm can be applied to the nonlinear model to obtain on-line estimates of the paste thickness, non-Newtonian behavior ($b'_2$), and friction. Note, however, that this estimation scheme is a two step process and material estimates are obtained separately from the friction coefficient. But by frequently repeating the two step estimation process, all unknown parameters can be determined in real time.

The following sections will describe the details of the estimation algorithms. Experimental results for both the linear and nonlinear model are presented.

## 5.2   Least Squares Estimation

For systems in which measurable and other known quantities are linearly related by unknown paramters, the least squares method provides the optimal solution for parameter estimation. Using this method, the unknown parameters are estimated such that the square of the error between the actual system output $y(t)$, and estimated system output $\hat{y}(t)$, is a minimum.

The notation frequently used in textbooks on the subject of parameter estimation

[32] would write Equation 5.1 in the form

$$y(t) = \phi_1(t)\theta_1 + \phi_2(t)\theta_2 + \cdots + \phi_n(t)\theta_n = \phi(t)^T\theta \qquad (5.6)$$

where $y(t)$ is the observation at time $t$, $\phi_n$ are referred to as regressors, and $\theta_n$ are unknown factors to estimate. For the linear model of the printing operation given by Equation 5.1, $y(t) = F_x$, $\phi_{1,2,3} = V_{sq}$, $F_y$, and 1, and the unknown parameters $\theta_i = b_i$.

Defining $V(\theta, t)$ as the sum of the squares of error by

$$V(\theta, t) = \frac{1}{2}\sum_{i=1}^{t}\varepsilon(i)^2 \qquad (5.7)$$

where $\varepsilon$ is given as

$$\varepsilon(i) = y(i) - \phi^T(i)\theta \qquad (5.8)$$

we obtain,

$$V(\theta, t) = \frac{1}{2}\sum_{i=1}^{t}\left(y(i) - \phi^T(i)\theta\right)^2 = \frac{1}{2}E^T E \qquad (5.9)$$

where $E = Y - \Phi\theta$ and $Y(t) = [y(1), y(2) \cdots y(t)]^T$. $\Phi$ is the matrix containing the regressor data from $t = 1$ to $t$. Since the expression for squared error $V(\theta, t)$ is quadratic, a solution which minimizes this function can be determined by completing the square. When this operation is performed, the squared error can be written as,

$$
\begin{aligned}
2V(\theta, t) &= Y^T\left(I - \Phi(\Phi^T\Phi)^{-1}\Phi^T\right)Y \\
&\quad + \left(\theta - (\Phi^T\Phi)^{-1}\Phi^T Y\right)^T \Phi^T\Phi\left(\theta - (\Phi^T\Phi)^{-1}\Phi^T Y\right)
\end{aligned} \qquad (5.10)
$$

Only the second term of Equation 5.10 is a funtion of $\theta$. Furthermore this term is always positive. The solution, therefore, which minimizes the squared error in Equation 5.10 is,

$$\theta = \hat{\theta} = \left(\Phi^T\Phi\right)^{-1}\Phi^T Y \qquad (5.11)$$

Notice that the term $\left(\Phi^T\Phi\right)^{-1}$ must be nonsingular for a solution to exist. This term is called the *covariance matrix*, denoted by $P(t)$ and represents the uncertainties of

47

the estimated parameters. The expression $\left(\Phi^T \Phi\right)^{-1} \Phi^T$ is called the *pseudoinverse* of $\Phi$. The condition that $\left(\Phi^T \Phi\right)^{-1}$ be nonsingular is the notion of persistent excitation. That is, to minimize the squared error between the measured output $y(t)$ and estimated output $\hat{y}(t) = \phi^T \hat{\theta}$, the system must be persistently excited for $\hat{\theta}$ to converge to the actual system parameters. Satisfaction of the excitation condition ensures that data gathered over a broad range will lead to an optimal solution for $\hat{\theta}$, assuming the linear model is valid.

## 5.2.1   Recursive Least Squares Estimation

For systems in which data is sampled and examined sequentially, techniques for updating the parameters based on incoming data are useful. The least squares algorithm can be extended to recursive computations. A benefit of the recursive method is rapid convergence, an essential requirement if any system is to implement the estimation scheme on-line.

An initial covariance matrix $P_0$ is chosen to represent the initial uncertainty in the parameters $\theta_i$. This matrix must be positive definite and usually is chosen with large initial diagonal entries. At time step (t+1), the estimated parameters $\hat{\theta}(t+1)$, and covariance matrix $P(t + 1)$ are updated. The recursive computations are,

$$\hat{\theta}(t) = \hat{\theta}(t-1) + K(t)\left(y(t) - \phi^T(t)\hat{\theta}(t-1)\right) \tag{5.12}$$

$$K(t) = P(t)\phi(t) \tag{5.13}$$

$$P(t) = P(t-1) - P(t-1)\phi(t)\left(I + \phi^T P(t-1)\phi(t)\right)^{-1} \tag{5.14}$$

The algorithm is said to have converged when the elements of the covariance matrix are a minimum. An example of how the recursive least squares algorithm operates is shown in Figure 5-1 for a simple linear system in the presence of random noise. Note that after approximately 40 iterations of the algorithm, $\hat{\theta}_i = \theta_i$. Convergence to the true values of $\theta_i$ is rapid even in the presence of noise, which was intentionally added to the simulated output $y(t)$.

However, the parameters in the model given in Figure 5-1 are time invariant,
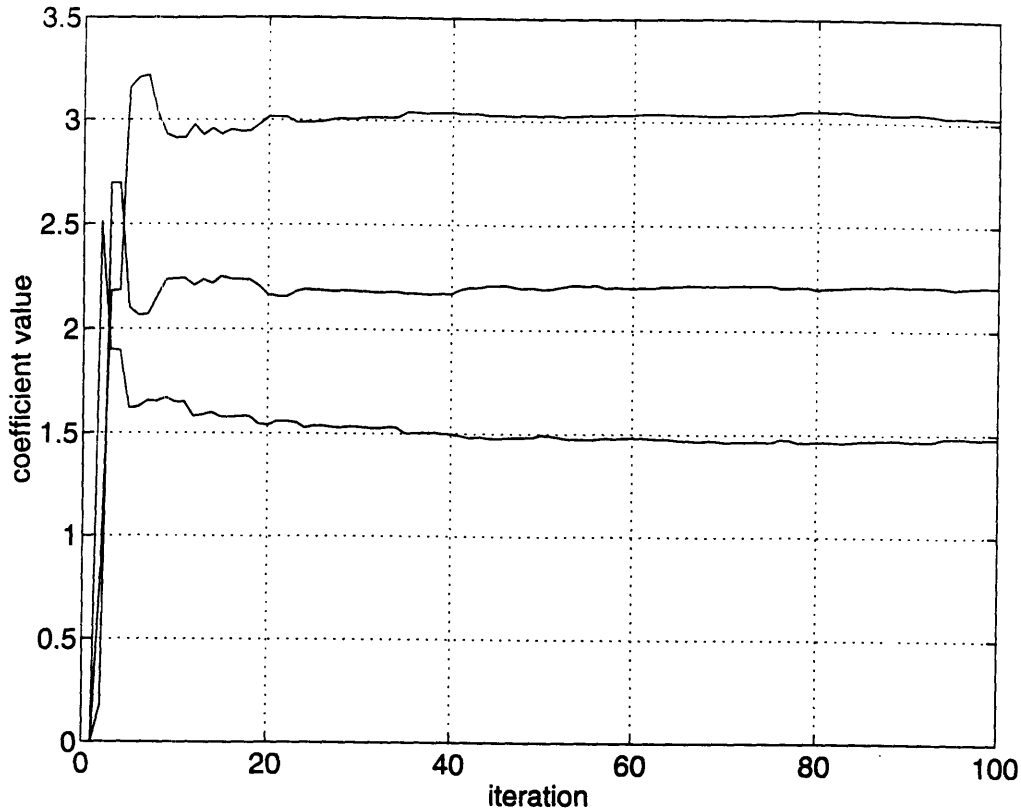
Figure 5-1: Simulation of the recursive least squares algorithm for a system with constant coefficients. $y = 1.5\phi_1 + 2.2\phi_2 + 3.0\phi_3 + noise$

which is not the case for stencil printing. Paste properties vary due to shear thinning and solvent evaporation. Standard recursive methods are not sufficient for tracking parameters which vary with time because the entire time history of data is reflected in the covariance matrix. Windowing techniques for evaluating the most recent data should be used for the case of time varying systems. An exponentially weighted algorithm can be used and is the subject of the following section.

## Exponential Forgetting and Covariance Resetting

The recursive computation described above assumes that the parameters are time invariant which may lead an erroneous solution for the unknown parameters, as shown in Figure 5-2. The estimates which are not tracking the varying parameters are those obtained by the standard recursive technique in section 5.2.1, while superior tracking is accomplished by exponentially forgetting old data. *Exponential forgetting* slightly modifies the standard recursive algorithm, such that old data is discarded and the
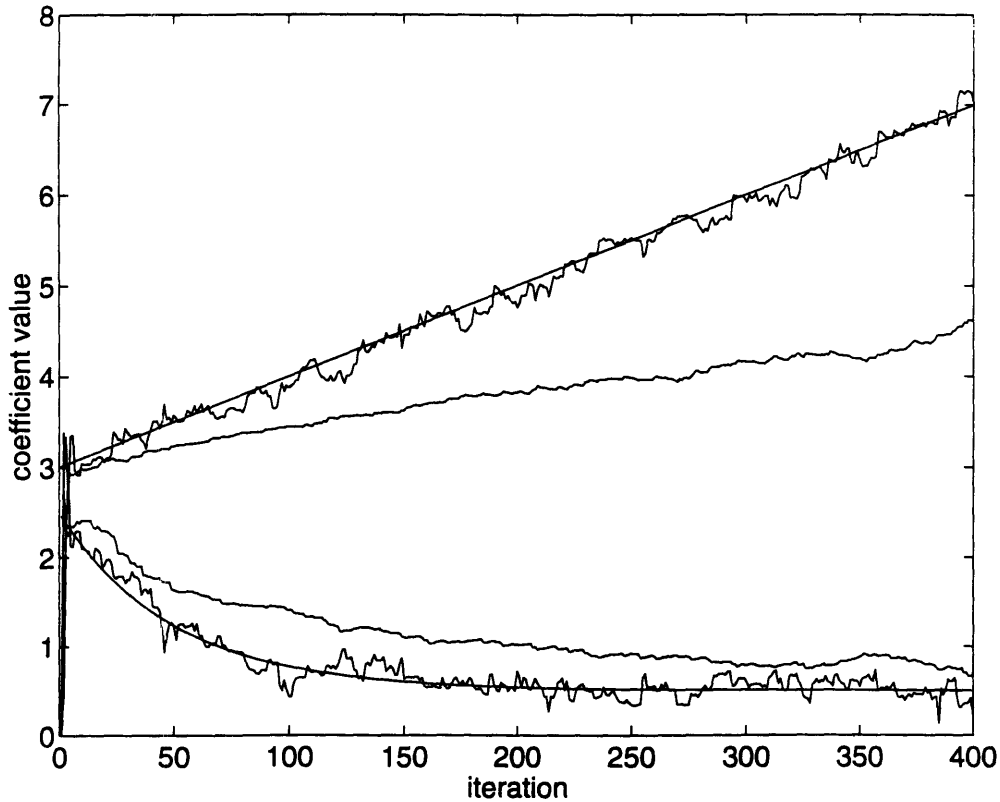
49

Figure 5-2: Comparison of the estimation algorithm with exponential forgetting $\lambda = 0.7$ and $\lambda = 1.0$ (no forgetting).

most recent information is used to identify the system parameters. A new error function is defined by,

$$V(\theta, t) = \frac{1}{2} \sum_{i=1}^{t} \lambda^{t-i} \varepsilon(i)^2 \tag{5.15}$$

where $\lambda$ is a *forgetting factor* and $0 < \lambda \leq 1$. The equations which minimize this error function is,

$$\hat{\theta}(t) = \hat{\theta}(t-1) + K(t)\left(y(t) - \phi^T(t)\hat{\theta}(t-1)\right) \tag{5.16}$$

$$K(t) = P(t)\phi(t) = P(t-1)\phi(t)\left(\lambda I + \phi^T P(t-1)\phi(t)\right)^{-1} \tag{5.17}$$

$$P(t) = \frac{\left(I - K(t)\phi^T(t)\right) P(t-1)}{\lambda} \tag{5.18}$$

As previously mentioned, better estimation performance is accomplished using exponential forgetting in the presence of time varying parameters as shown in Figure 5-2. However, this technique also has limitations. Specifically, the forgetting factor $\lambda$ is a

constant, but should rather depend on the rate of change of plant behavior. On one hand, when there is no source of fluctuation, $\lambda$ should approach unity, in which case forgetting collapses to the standard recursive least squares algorithm. On the other hand, rapid shifts should use a forgetting factor with small values. Obsolete information should be discarded as quickly as possible, but the estimation method must maintain some memory to achieve reasonable tracking. Since the viscosity breakdown of solder paste is characterized by a long time constant relative to the sampling time of the printer, exponential forgetting is an appropriate choice for on-line monitoring of the printing operation.

When there is an abrupt change in system characteristics, the exponentially weighted forgetting factor is still useful, although it is best suited to compensate for slow drifts. A discrete event indicates a large uncertainty in parameter values. This sudden uncertainty should be reflected in the covariance matrix by resetting the covariance matrix to a new initial state. Simulation of the exponential forgetting algorithm and the combination of forgetting and covariance resetting is shown in Figure 5-3.

## 5.3   Results During Printing

The recursive least squares algorithm with exponential forgetting was implemented for estimation of the unknown parameters for both the linear model of Equation 5.1 and the nonlinear model, Equation 5.2, using data collected during the printing operation.

### 5.3.1   Estimation for the Linear Model

The results of the estimation algorithm for three different pastes are as shown in Figures 5-4 through 5-6, using the linear system described by Equation 5.1. The data shown was acquired during the printing cycles of twenty PCB's. Single direction printing was used in all tests over the linear region for squeegee speeds between 5 and 10 $cm/s$. From these graphs, it is clear that the estimates track the shear thinning behavior for the duration of experiments.
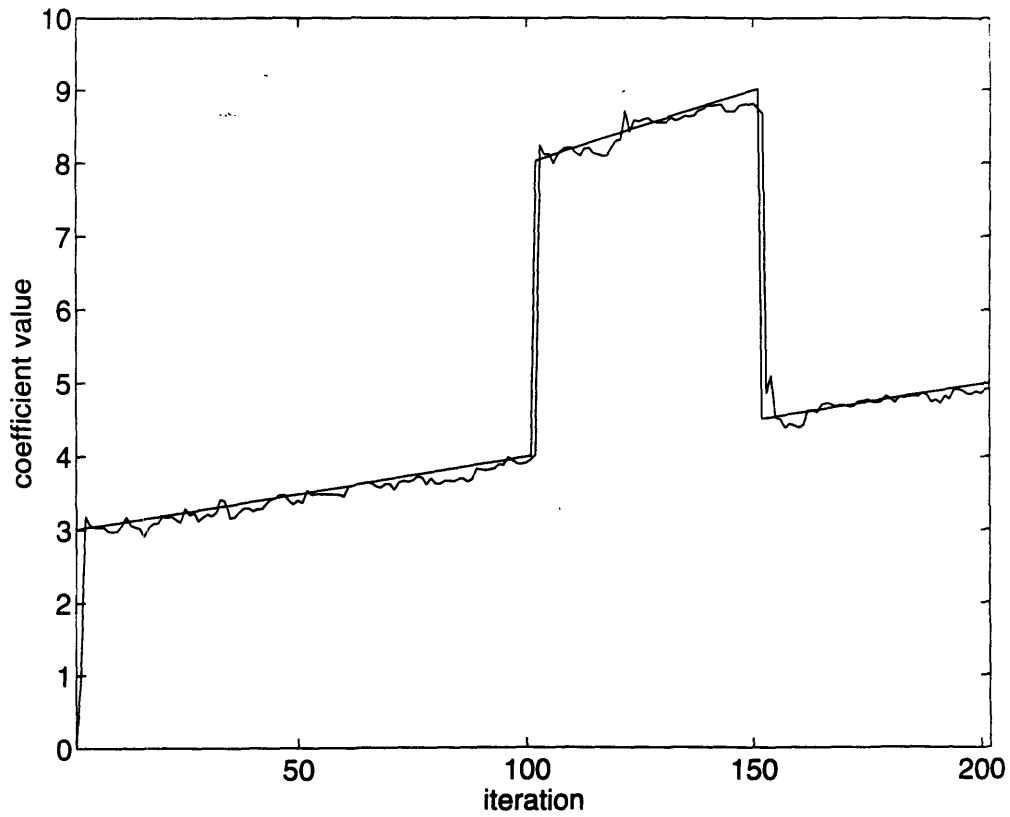
Figure 5-3: In the presence of a discrete change to the system, covariance resetting in combination with exponential forgetting converged faster than by forgetting alone.
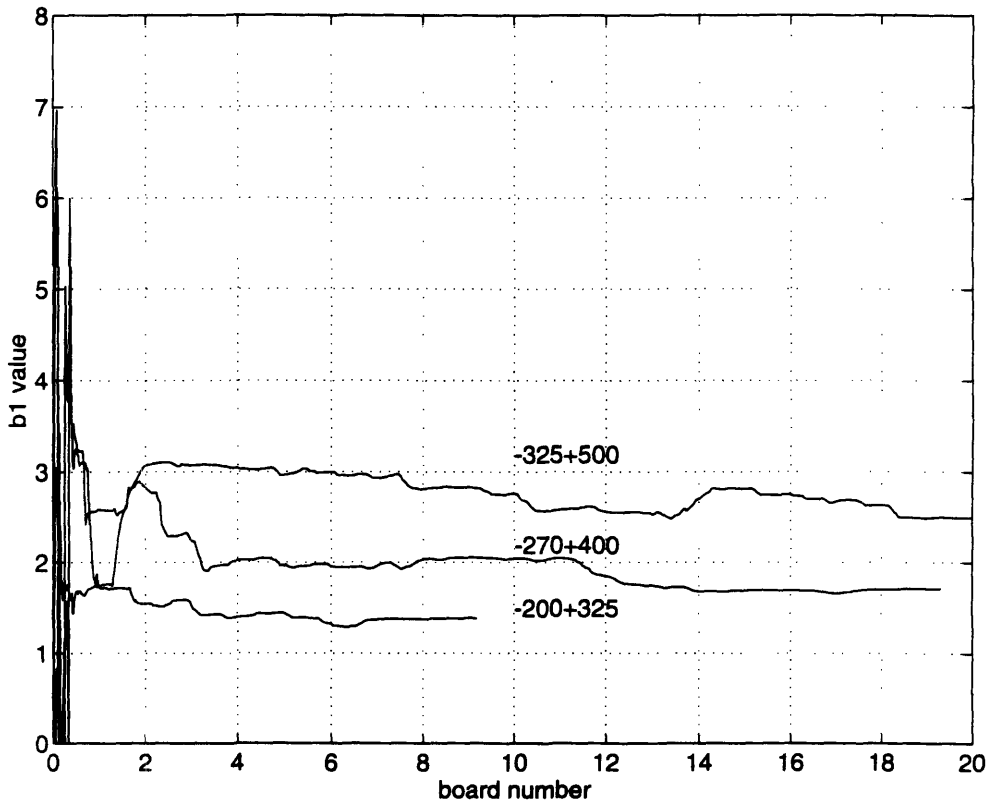


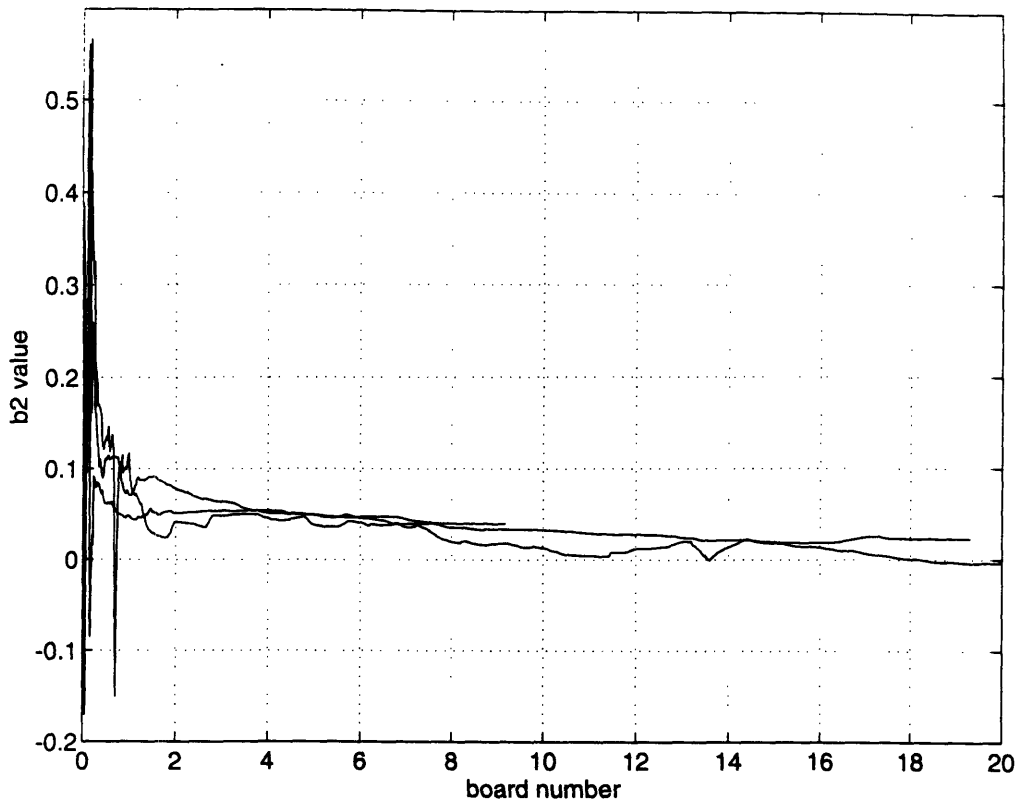Figure 5-4: Parameter estimates for $b_1$ for three solder pastes.

Figure 5-5: Parameter estimates for $b_2$ for three solder pastes.


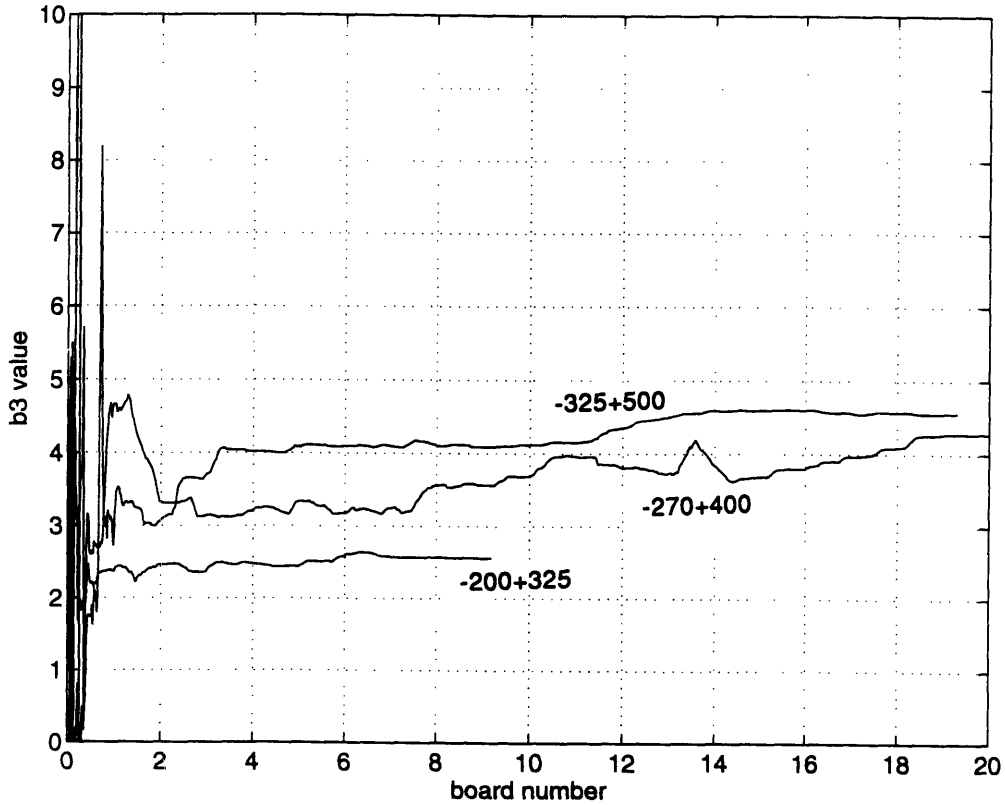
-325+500

-270+400

-200+325

Figure 5-6: Parameter estimates for $b_3$ for three solder pastes.

Since the current printing machine was not equipped with downward force or squeegee velocity actuators, the persistent excitation condition was satisfied by manually adjusting $V_{sq}$ and $F_y$ during the print cycles. When implemented on a printing machine with actuation capabilities, convergence will occur within the first few centimeters of squeegee travel. Rapid convergence is important for this technique to be applied to the printing process on-line. To satisfy this requirement, the excitation and estimation routine can be conducted over a region in front of and beyond the print pattern. In doing so, the actual depositions will not be disturbed by varying machine conditions during the printing operation.

## 5.3.2  Nonlinear Model Estimation

The results obtained for the linear model were able to detect the time dependent behavior of the paste. Long term shear thinning was observed and pronounced changes in fluid behavior were recorded as a function of print direction. These results are useful, but it should be emphasized that they are only meaningful if the estimates of the coefficients are obtained within a linear region. That is, for results to be consistent, the condition of persistent excitation must be satisfied over a limited linear region of the $F_x$, $V_{sq}$ curve. Because this curve can be approximated as piecewise linear, different values for $b_1$ and $b_2$ will be estimated depending on the operating region of the squeegee, as demonstrated in Figure 5-7.

Qualitatively, as the squeegee speed increases, the slope of the approximated line will decrease and the intercept will increase. Mathematically, the slope of the curve can be calculated by differentiating the power law expression given in Equation 2.3. Neglecting friction, the following relationship is obtained for the slope,

$$\frac{dF_x}{dV_{sq}} = b_1' b_2' V_{sq}^{(b_2' - 1)}$$

(5.19)

By direct substitution of Equation 5.19 for $b_1$ in the linear model, Equation 5.1, a relationship among the linear model's slope, intercept, and power law coefficients can
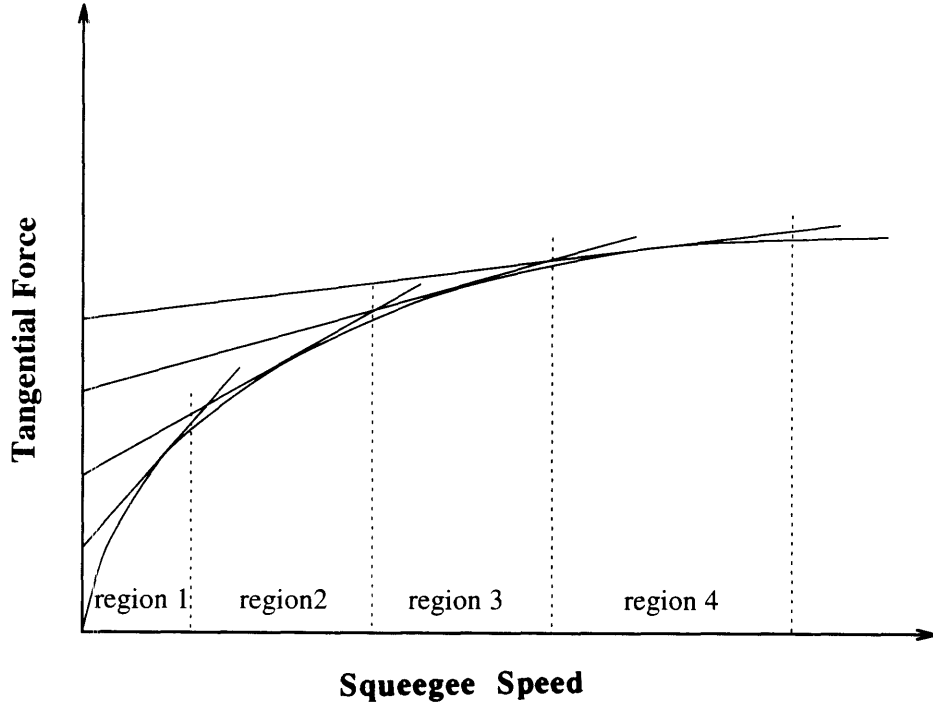
54

Figure 5-7: Piecewise linear approximation of the $V_{sq}$, $F_x$ curve.

be derived. This expression is given by,

$$b_3 = b_1'(1 - b_2')\left(\frac{b_1}{b_1' b_2'}\right)^{\left(\frac{b_2'}{b_2'-1}\right)} \qquad (5.20)$$

Recall that $b_2' = n$, the exponent for the power law, and in this case is always less than 1. Similarly, $b_1' = k$ for the power law. The curve fit shown in Figure 4-4 for a -325+500 paste was calculated having $k = 1.86$ and $n = 0.27$. Substituting these into Equation 5.20, it is clear that the linear model slope $b_1$ varies as the inverse of $b_3^3$. Notice that for $n = 0.5$, $b_1$ and $b_3$ will be inversely proportional. This dependence of the parameters was observed when the squeegee speed was varied over too broad a range, hence including regions with more pronounced nonlinear behavior. Real time estimation data detailing the $b_1$, $b_3$ dependence is shown in Figure 5-8.

The dependence of the slope and intercept terms was an important observation. In an on-line setting, the exact shape of the curve relating $F_x$ and $V_{sq}$ for any paste is not known *a priori*; hence, the allowable range of squeegee speeds over which the
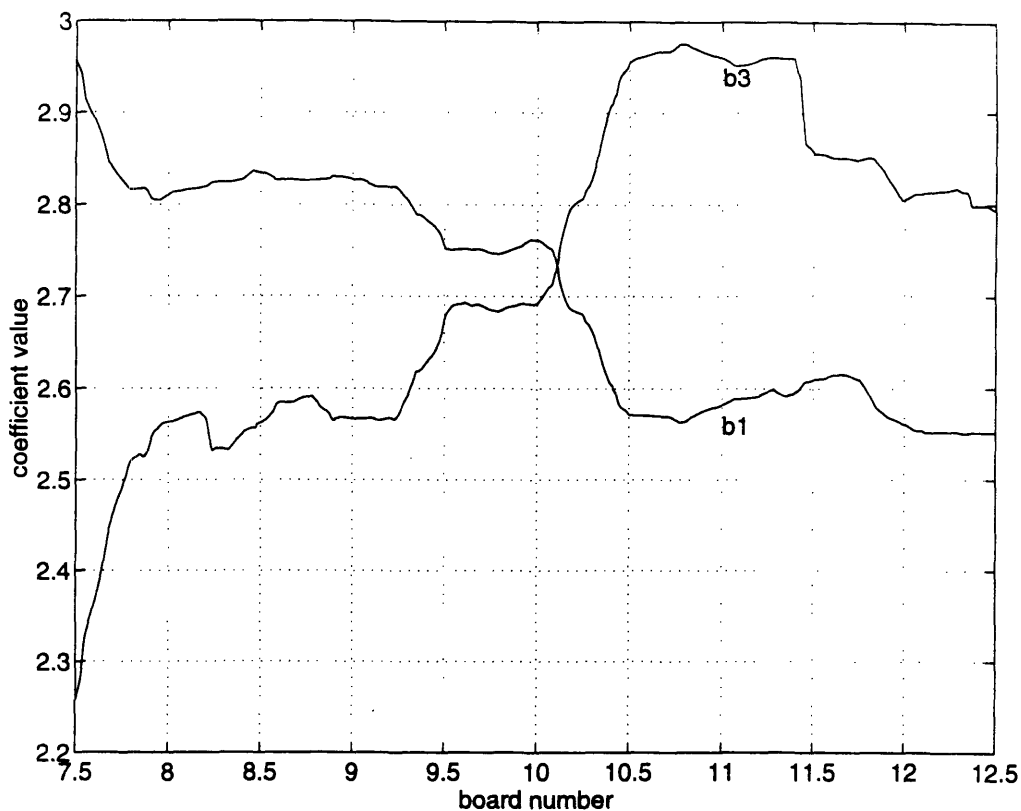
Figure 5-8: $b_1$ varies approximately as the inverse of $b_3^3$ for a power law exponent of $n = 0.27$.

linear model is valid is unknown. The limited range over which the system can be excited is uncertain, and changes observed in the model parameters may strictly be due to system nonlinearities. For this reason, estimates of the parameters involved in the nonlinear model, $b_i'$, may prove more valuable for characterizing the fluid behavior. The linear model is restricted to *local* phenomenon, while the parameters of the nonlinear model contain more *global* information.

Estimates of the power law coefficients for different solder pastes using the nonlinear model of Equation 5.2 are shown in Figures 5-9 through 5-10. The corresponding power law curves for the estimated $b_i'$ of the -325+500 paste are shown in Figure 5-11.
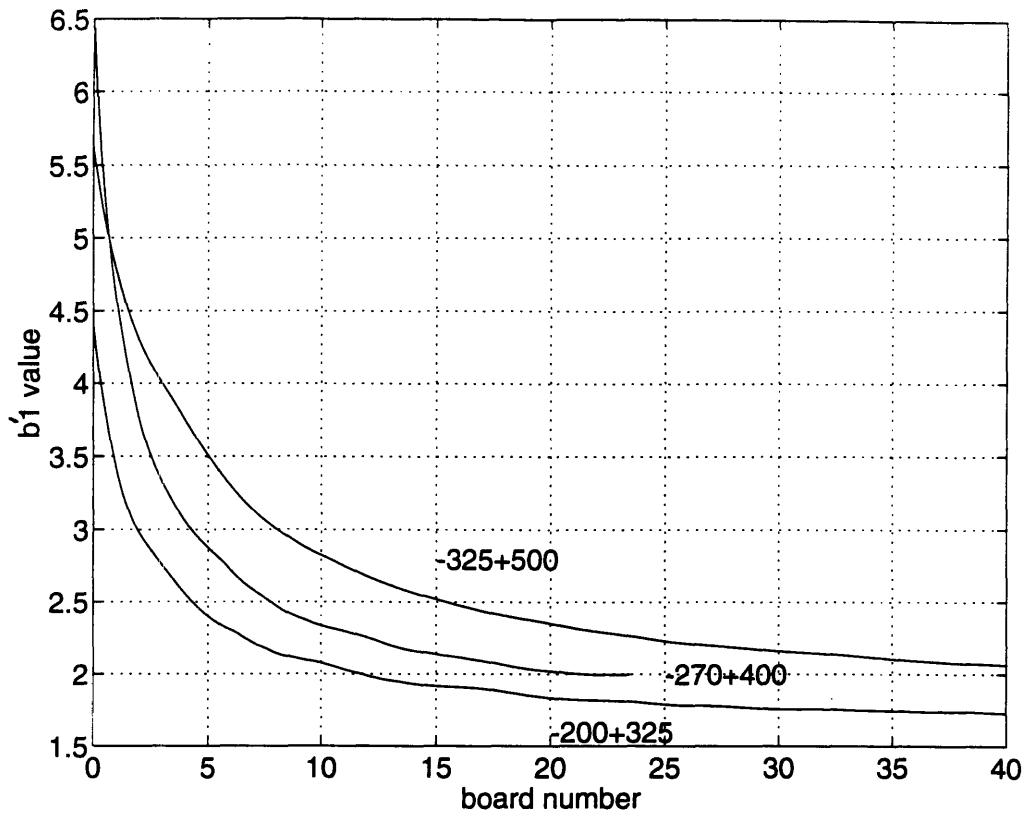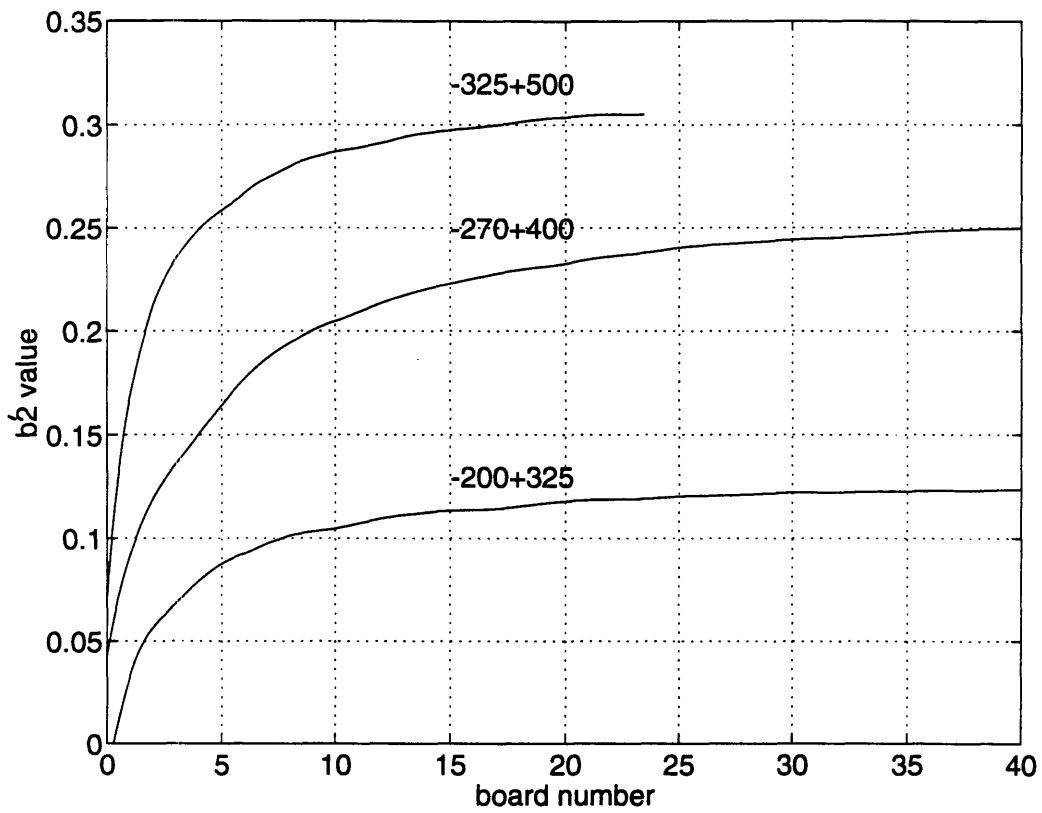
Figure 5-9: Estimates of the $k$ terms, $b_1'$.



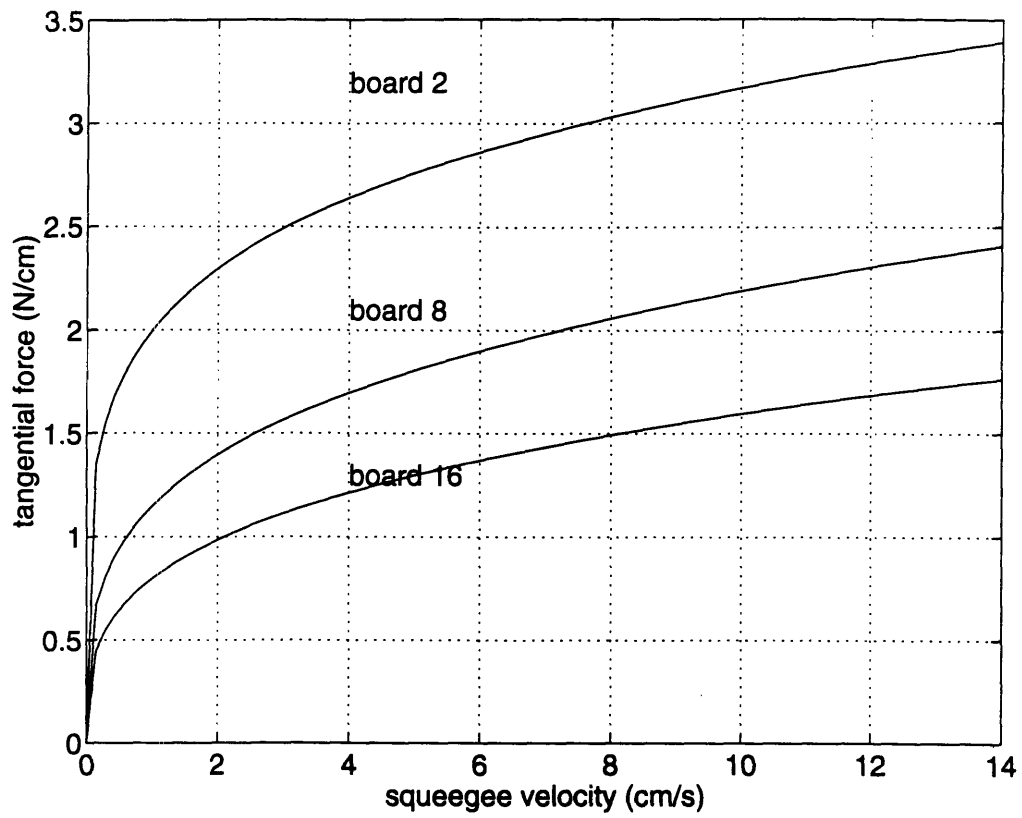Figure 5-10: Estimates of the $n$ terms, $b_2'$.

Figure 5-11: Power law curves using estimated $b_i'$ after 16 prints.

# Chapter 6

# Conclusions and Future Work

The development of ultra fine pitch surface mount devices has prompted many researchers in the electronic packaging industry to focus their attention to the application of solder paste onto printed circuit boards. Despite these efforts, however, there has remained a significant mismatch between the theoretical models of the fluid mechanics and the application of these models for process improvement. Presumably, a model should be used for process improvement and control, in which case, paste properties must be monitored on-line. Explicit relationships involving the properties' dependence on temperature, humidity, work, and time do not need to be derived if the relevant properties can be estimated directly from *in-situ* measurements. On-line material estimation was the primary goal of this research.

The control of hydrodynamic pressure is critical if deposits of uniform height are to be produced. To satisfy this requirement, attention was directed toward the modeling of solder paste motion by squeegee action. Beginning with Navier-Stokes equations for viscous, low Reynolds number flow, equations for the hydrodynamic forces acting on the face of the squeegee were derived, using the streamline solution by [10]. By balancing forces acting on the squeegee, a linear model was developed in which measurable quantities and actuated signals were linearly related by parameters which characterized paste viscosity and the stencil/squeegee interface. The consequence of this linear involvement was that recursive least squares algorithms could be implemented to estimate the model parameters in real time.

The Newtonian assumption was tested using data acquired from the printing machine, and found that over a limited working range of squeegee speeds, the $F_x, V_{sq}$ behavior was linear. This indicated that for small ranges of squeegee speeds, the dominant fluid shear rates were linearly related to the stresses. Furthermore, an empirically derived power law model was used to describe the nonlinearities, hence characterizing the fluid behavior over a broad working range. Through algebraic manipulation, the power law model was recast into a linear form so that recursive least squares techniques could be applied.

Experimental estimation data were presented for both the linear and nonlinear models. While the linear model may provide useful results for *local* phenomena, the parameters involved in the nonlinear model characterize *global* behavior of the paste.

At this point, it is unclear which model provides the most useful data, since no research has yet been conducted relating measurements of actual paste deposits to machine settings, force measurements, and parameter estimates. We may speculate that the nonlinear model provides more useful results since it characterizes *global* fluid behavior. The flow into the stencil apertures will undoubtedly undergo different rates of shear than the flow during rolling motion. Since this will be the case, the parameter estimates of the linear model may not provide sufficient information regarding aperture flow. Correlation of parameter estimates, machine settings, and force measurements to paste height data is the subject of current research. Once a model is developed for the flow into the stencil apertures, data can be used from both post process inspection and *in-situ* measurements for dynamic control of the process parameters. Issues pertaining to the development of closed loop control algorithms utilizing both continuous feedback through in-process sensors and information acquired from discrete inspection events are currently being addressed.

# Bibliography

[1] Gerald Ginsberg. *Surface Mount and Related Technologies*. Marcel Dekker, Inc., 1989.

[2] John W. Evans and John Keith Beddow. Characterization of particle morphology and rheological behavior in solder paste. *IEEE Transactions on Components, Hybrids, and Manufacturing Technology*, 10(2):224–231, June 1987.

[3] R.E. Trease and R.L. Dietz. Rheology of pastes in thick film printing. *Solid State Technology*, 15(1):39–43, 1972.

[4] B. Rooz-Kozel. Solder pastes. *Surface Mount Technology*, 1984.

[5] Shigeyuki Ogata. Rheology and printability of solder paste. *IEICE Transactions*, E74(8), August 1991.

[6] Nobuo Kamada. Fine-pitch patterns prompt adjustments in solder paste printing. *JEE*, May 1993.

[7] C.R. Herman, V.A. Skormin, and G.R. Westby. Application of impedance spectroscopy for on-line monitoring of solder paste. *ASME Transactions, Journal of Electronic Packaging*, 115:44–54, March 1993.

[8] Martin A. Seitz, Richard W. Hirthe, Mohammad N. Amin, and Mark H. Polczynski. Monitoring solder paste properties using impedance spectroscopy. In *ISHM Proceedings*, pages 503–509, 1992.

[9] Sir Geoffrey I. Taylor. Similarity solutions of hydrodynamic problems. In Nicholas John Hoff and Walter Guido Vincenti, editors, *Aeronautics and Astronautics, Proceedings of the Durand Centennial Conference*, pages 21–28, 1960.

[10] Sir Geoffrey I. Taylor. On scraping viscous fluid form a plane surface. In *The Scientific Papers of Sir Geoffrey Ingram Taylor*, pages 410–413. Cambridge University Press, 1971.

[11] T.F. Hanrahan, P.F. Monaghan, and R.D. Babikian. Modeling of a solder paste flow with a free surface in stencil printing. In *ASME/JSME Conference on Electronics Packaging*, pages 587–592, 1992.

[12] Joseph Kedra. Estimation of shear rates during rolling in the screening and stencilling process. *International Journal for Hybrid Microelectronics*, 12(4):188–194, December 1989.

[13] Jerzy A. Owczarek and Frank L. Howland. A study of the off-contact screen printing process : Part 1: Model of the process and some results derived from experiments. *IEEE Transactions on Components, Hybrids, and Manufacturing Technology*, 13(2):358–367, June 1990.

[14] Jerzy A. Owczarek and Frank L. Howland. A study of the off-contact screen printing process: Part 2: Analysis of the model of the printing process. *IEEE Transactions on Components, Hybrids, and Manufacturing Technology*, 13(2):368–375, June 1990.

[15] Burke Hunter. A simplified analysis of blade coating with applications to the theory of screen printing. *International Journal for Hybrid Microelectronics*, 12(2):88–94, June 1989.

[16] Dietrich E. Riemer. Analytical engineering model of the screen printing process: Part 1. *Solid State Technology*, pages 107–111, August 1988.

[17] Dietrich E. Riemer. Analytical engineering model of the screen printing process: Part 2. *Solid State Technology*, pages 85–90, August 1988.

[18] S.H. Mannan, N.N. Ekere, E.K. Lo, and I. Ismail. Application of ink screening models to solder paste printing in smt assembly. *Journal of Electronics Manufacuring*, 3:113–120, 1993.

[19] G. Caswell and J.D. Marcy. *Surface Mount Technology*. The International Society for Hybrid Microelectronics, 1984.

[20] C.A. Lea. *A Scientific Guide to Surface Mount Technology*. Electromechanical Publications Limited, 1988.

[21] R. Byron Bird, Robert C. Armstrong, and Ole Hassager. *Dynamics of Polymeric Liquids*, volume 1. John Wiley and Sons, 1977.

[22] W.A. Wilkenson. *Non-Newtonian Fluids*. Pergamon Press, 1960.

[23] W.E. Langlois. *Slow Viscous Flow*. Macmillan Press, 1964.

[24] W.R. Dean and P.E. Montagnon. On the steady motion of viscous liquid in a corner. *Proceedings of The Cambridge Philosophical Society*, 45:389–394, 1949.

[25] H.K. Moffatt. Viscous and resistive eddies near a shrp corner. *Journal of Fluid Mechanics*, 18:1–18, 1964.

[26] C. Hancock, E. Lewis, and H.K. Moffatt. Effects of inertia in forced corner flow. *Journal of Fluid Mechanics*, 112:315–327, 1981.

[27] Gareth H. McKinley, William P. Raiford, Robert A. Brown, and Robert C. Armstrong. Nonlinear dynamics of viscoelastic flow in axisymmetric abrupt contractions. *Journal of Fluid Mechanics*, 223:411–455, 1991.

[28] Michael Renardy. The stresses of an upper convected maxwell fluid in a newtonian velocity field near a re-entrant corner. *Journal of Non-Newtonian Fluid Mechanics*, 50(2-3):127–134, 1993.

[29] E.J. Hinch. The flow of an oldroyd fluid around a sharp corner. *Journal of Non-Newtonian Fluid Mechanics*, 50(2-3):161–171, 1993.

[30] P. Henriksen and O. Hassager. Corner flow of power law fluids. *Journal of Rheology*, 33(6):865–879, 1989.

[31] R.T. Fenner. On local solutions to non-newtonian slow viscous flow. *International Journal of Non-Linear Mechanics*, 10:207–214, 1975.

[32] G.C. Goodwin and K.S. Sin. *Adaptive Filtering Prediction and Control.* Prentice Hall, 1984.